Received 2002 July 1; accepted 2003 June 1
Preprint typeset using LaTeX style emulateapj v. 7/15/03

GALAXY FORMATION: CDM, FEEDBACK AND THE HUBBLE SEQUENCE

Jesper Sommer-Larsen, Martin Götz and Laura Portinari
Theoretical Astrophysics Center, Juliane Maries Vej 30, DK-2100 Copenhagen Ø, Denmark

Received 2002 July 1; accepted 2003 June 1

ABSTRACT

TreeSPH simulations of galaxy formation in a standard ΛCDM cosmology, including star formation, effects of energetic stellar feedback processes and of a meta-galactic UV field have been performed, resulting in a mix of realistic disk, lenticular and elliptical galaxies at redshift z=0.

The disk galaxies are deficient in angular momentum by only about a factor of two compared to observed disk galaxies for simulations with fairly strong star-bursts in early, proto-galactic clouds, leading to "blow-away" of the remaining gas in the clouds. In this respect the present scenario is hence doing almost as well as the WDM scenarios discussed by Sommer-Larsen & Dolgov. The surface density profiles of the stellar disks are approximately exponential and those of the bulges range from exponential to $r^{1/4}$, as observed. The bulge-to-disk ratios of the disk galaxies are consistent with observations and likewise are their integrated B–V colours, which have been calculated using stellar population synthesis techniques. Furthermore, the observed I-band Tully-Fisher relation can be matched, provided that the stellar mass-to-light ratio of disk galaxies is $M/L_I \sim 0.8$, similar to what was found by Sommer-Larsen & Dolgov from their WDM simulations and in fair agreement with several recent observational determinations of M/L_I for disk galaxies.

The ellipticals and lenticulars have approximately $r^{1/4}$ stellar surface density profiles, are dominated by non disk-like kinematics and flattened due to non-isotropic stellar velocity distributions, again consistent with observations.

Hot halo gas is predicted to cool out and be accreted onto the Galactic disk at a rate of 0.5–1 $M_\odot$/yr at z=0, consistent with upper limits deduced from *FUSE* observations of OVI. We have analyzed in detail the formation history of two disk galaxies with circular speeds comparable to that of the Milky Way and find gas accretion rates, and hence bolometric X-ray luminosities of the haloes, 6–7 times larger at $z \sim 1$ than at z=0 for these disk galaxies. More generally, it is found that gas infall rates onto these disks are nearly exponentially declining with time, both for the total disk and the "solar cylinder". This theoretical result hence supports the exponentially declining gas infall approximation often used in chemical evolution models. The infall time-scales deduced are ∼5–6 Gyr, comparable to what is adopted in current chemical evolution models to solve the "G-dwarf problem".

The disk of one of the two galaxies forms "inside-out", the other "outside-in", but in both cases the mean ages of the stars in the outskirts of the disks are $\gtrsim$6–8 Gyr, fairly consistent with the findings of Ferguson & Johnson for the disk of M31.

The amount of hot gas in disk galaxy haloes is consistent with observational upper limits. The globular cluster M53 and the LMC are "inserted" in the haloes of the two Milky Way like disk galaxies and dispersion measures to these objects calculated. The results are consistent with upper limits from observed dispersion measures to pulsars in these systems.

Finally, the results of the simulations indicate that the observed peak in the cosmic star formation rate at redshift $z \sim 2$ can be reproduced. Depending on the star formation and feedback scenarios one predicts either a cosmic star formation rate which decreases monotonically with redshift beyond these redshifts or a second peak at z∼6–8 corresponding to the putative population III, and interestingly similar to recent estimates of the redshift at which the Universe was reionized. These various scenarios should hence be observationally constrainable with upcoming instruments like JWST and ALMA.

Subject headings: cosmology: theory — dark matter — galaxies: formation — galaxies: evolution — galaxies: structure — methods: numerical

1. INTRODUCTION

The formation of galactic disks is one of the most important unsolved problems in astrophysics today. In the currently favored hierarchical clustering framework, disks form in the potential wells of dark matter haloes as the baryonic material cools and collapses dissipatively. It has been shown (Fall & Efstathiou 1980) that disks formed in this way can be expected to possess the observed amount of angular momentum (and therefore the observed spatial extent), but only under the condition that the infalling gas retains most of its original angular momentum — see also Fall (2002).

Numerical simulations of this collapse scenario in CDM cosmologies, however, have so far consistently indicated that, when only radiative cooling processes are included, the infalling gas loses too much angular momentum (by more than an order of magnitude) and the resulting disks are accordingly much smaller than required by the observations (e.g., Navarro & Benz 1991; Navarro & White 1994; Navarro, Frenk, & White 1995; Navarro & Steinmetz 1997 using N-body/SPH codes and Bryan

2003 using an Adaptive Mesh Refinement code, Bryan 1999). This discrepancy is known as the *angular momentum problem* of disk galaxy formation. It arises from the combination of the following two facts: a) In the CDM scenario the magnitude of linear density fluctuations $\sigma(M) =< (\delta M/M)^2 >^{1/2}$ increases steadily with decreasing mass scale M leading to the formation of non-linear, virialized structures at increasingly early epochs with decreasing mass, i.e. the hierarchical "bottom-up" scenario. b) Gas cooling is very efficient at early times due to gas densities being generally larger at higher redshifts, as well as the rate of inverse Compton cooling also increasing very rapidly with redshift ($\propto (1+z)^4$). a) and b) together lead to rapid condensation of small, dense gas clouds, which subsequently lose energy and (orbital) angular momentum by dynamical friction against the surrounding dark matter halo before they eventually merge to form the central disk. A mechanism is therefore needed that prevents, or at least delays, the collapse of small proto-galactic gas clouds and allows the gas to preserve a larger fraction of its angular momentum as it settles into the disk. Weil, Eke, & Efstathiou (1998) have shown that if the early radiative cooling is suppressed (by whatever means), numerical simulations can indeed yield more realistically sized disks — see also Eke, Efstathiou & Wright (2000). The physical mechanism by which cooling is suppressed or counteracted, however, was not specified.

Sommer-Larsen et al. (1999, hereafter SLGV99) discussed the effects of various stellar reheating mechanisms in more detail using numerical TreeSPH simulations of disk galaxy formation in the SCDM cosmology. They found that reheating of the Universe resulting from more or less *uniformly* distributed star formation does not lead to a solution to the angular momentum (AM) problem, but that localized star-bursts in proto-galactic gas clouds might: *if* the star-bursts can blow the remaining bulk part of the gas out of the small and dense dark matter haloes associated with the clouds, then test simulations showed that the gas later settles gradually forming an extended, high angular momentum disk galaxy in the central parts of a large, common dark matter halo. The physics of global gas blow-out processes were considered in early calculations by Dekel & Silk (1986) and Yoshii & Arimoto (1987), indicating that star-bursts might well blow out most of the gas in small galaxies with characteristic circular speed (defined in this paper as the circular speed in the disk at 2.2 exponential scalelengths) $V_c \lesssim 100$ km/s. More recent, detailed simulations by Mac Low & Ferrara (1999) suggest that this global blow-out scenario may not work so well in *disk* galaxies, even in small ones: the star-bursts typically lead to bipolar outflows of very hot gas perpendicular to the disk of the small galaxy, only expelling a minor fraction of the disk gas. This, however, is due to the particular geometry of a disk galaxy (the thinness and flatness of the disk); in a more roundish and bulky, proto-galactic dwarf galaxy, one would expect the energetic effects of star-bursts on the bulk of the dwarf galaxy gas to be much stronger.

It has proven difficult to realistically implement thermal energy feedback in cosmological N-body/SPH codes incorporating radiative cooling (Thacker & Couchman 2000 and references therein; Navarro & Steinmetz 2000; SLGV99). As first discussed by Katz (1992) this is mainly due to problems in resolving a multi-phase inter stellar medium (ISM) at the scales of individual star burst regions in cosmological simulations using SPH. It is also related to the smoothing of discontinuities in the thermodynamic variables inherent in the SPH method — some improvement on this, at least in relation to shocks, may be gained by replacing thermal energy by entropy as an independent variable in SPH (Springel & Hernquist 2002). In recent years, however, some progress has been made on the implementation of thermal energy feedback in SPH simulations (Gerritsen 1997; Mori et al. 1997; Thacker & Couchman 2000, 2001; Springel & Hernquist 2003 — see also Yepes et al. 1997; Ferrara & Tolstoy 2000; Lia, Portinari & Carraro 2002; Semelin & Combes 2002; Governato et al. 2002; Abadi et al. 2003 and Meza et al. 2003).

As was shown by Sommer-Larsen & Dolgov (2001, SLD01) by going from the CDM structure formation scenario to the warm dark matter (WDM) one can alleviate (and possibly even completely overcome) the AM problem without invoking effects of energetic feedback in the simulations at all (this does not imply, of course, that feedback necessarily *is* unimportant; it should rather be seen as a minimal assumptions approach). Fine-tuning of the warm dark matter particle mass to about 1 keV is required, however. In contrast, the salient feature about "conventional" CDM is that as long as the dark matter particles are much heavier than one keV, the actual particle mass does not matter for structure formation (note though, that axions, despite being ultra-light, behave like CDM).

In this paper we show how a mix of realistic disk, lenticular and elliptical galaxies[1] can be obtained in fully cosmological (ΛCDM), gravity/hydro simulations invoking star formation, energetic stellar feedback processes in early, proto-galactic clouds and a meta-galactic UV field. This is achieved by treating (albeit in a coarse way) the gas in regions where star-bursts are returning energy to the ISM as a two-phase medium, consisting of a "cold" ($T \sim 10^4$ K) and a hot ($T \sim 10^6$ K) component. Related, recent work includes Thacker & Couchman (2001), Steinmetz & Navarro (2002) and Springel & Hernquist (2003).

In section 2 the implementation of stellar feedback processes in the simulations is discussed. Section 3 gives a short presentation of the numerical code and the initial conditions. The simulations themselves are briefly described in section 4, and the results obtained are analyzed and discussed in section 5. Finally, in section 6 we summarize our conclusions and present a brief outlook.

2. STAR FORMATION AND STELLAR FEEDBACK

The star formation efficiency (SFE, defined as the ratio between the dynamical timescale and the star formation timescale — see below) in the Galactic disk is quite small at present, at most a few percent (e.g., Silk 1997). After extensive experimentation we have found that such a low SFE in combination with a "conventional" initial mass function (IMF) produces too low an energy feedback rate in the early and dense proto-galactic clouds to drive the remaining gas out of the (cold) dark matter potential

[1] Pictures of some of the galaxies can be seen at http://www.tac.dk/~jslarsen/Hubble_Sequence

wells in which they have formed. As a consequence, such a low SFE at early times does not lead to a solution of the AM problem for the CDM + feedback scenario - see section 5. A similar result was found by Abadi et al. (2003), but we note that Governato et al. (2002) found for one CDM galaxy formation simulation, that the AM problem could be solved (to within about a factor of two) using low, early SFE + feedback. In any case, for that scenario one is still faced with the problem that the stellar haloes become too massive (Governato et al. 2002) and/or the stellar spheroids too dominant and centrally concentrated (Abadi et al. 2003; Meza et al. 2003). Moreover, Governato et al. find for their CDM simulation that the number of stellar satellite galaxies is too large compared to observations of the Milky Way and M31 (the "missing satellites problem").

To solve the AM problem (to within about a factor of two; section 5) as well as the other problems mentioned above (section 5; Sommer-Larsen et al. 2003) we find that considerably larger energy feedback rates are required at early times. This can be achieved, for example, by invoking at early times 1) a considerably larger SFE or/and 2) a substantially more top-heavy IMF. In this paper, we shall not attempt to give a detailed, theoretical substantiation of these two possibilities, but a few, brief plausibility arguments can be given as follows:

The stars formed in the early, proto-galactic clouds will have low heavy element abundance, as they will belong to the first generations of stars formed in the Universe. Hence a physical motivation for case 1) could be related to the fact that the strength of stellar winds decreases with decreasing metallicity (Kudritzki et al. 1989; Kudritzki & Puls 2000), possibly with a sharp drop below metallicities of about 1/100 solar (Kudritzki 2002). So for *increasing* metal abundance, the stronger stellar winds may regulate star formation so as to *decrease* the SFE, due to the energy and momentum feedback to the star forming, molecular clouds. It is also possible that the SFE could depend on the thermal history of the gas such that gas which has been heated to temperatures well above T_{crit}~10^4 K (below which atomic radiative cooling becomes unimportant) and subsequently cooled down again has a lower SFE than gas which has never been heated above T_{crit}. Physically this could be related to a possible multi-phase structure of the former type of gas, effects of magnetic fields, destruction of molecules etc.

With respect to case 2) some theoretical work on star formation indicates that the IMF of the first generations of stars was in fact more top-heavy than present day IMFs (Abel, Bryan & Norman 2002; Bromm, Coppi & Larson 2002; and references in Chiosi 2000). Padoan & Nordlund (2002) find that the high-mass slope of the IMF becomes steeper at early times (when the magnetic fields in molecular clouds were considerably weaker than the $B \sim \mu$G at present), but also that the low-mass cut-off of the IMF at the same time increases considerably such as to effectively make their proposed IMF more top-heavy (or more appropriately "bottom-light") at early times (Å. Nordlund, 2002, private communication).

In this paper we consider case 1), but we have no reason to believe that case 2) would not work equally well.

We use two distinctly different star formation and feedback modes depending on the thermal history of the star forming gas (as chemical evolution is not yet implemented in the simulations):

- "Early" star formation mode

Cool, dense gas, which has *always* been cooler than $T_{crit} \simeq 10^4$ K is assumed to form stars rapidly, i.e. on a timescale comparable to the local, dynamical time t_{dyn}. We express this star formation timescale as

$$t_{*,e} = \frac{t_{dyn}}{\epsilon_e} = \frac{1}{(4\pi G\rho_{gas})^{1/2}}\frac{1}{\epsilon_e} \quad , \tag{1}$$

where the star formation efficiency $\epsilon_e \sim 1$ (we find that the specific value of ϵ_e used is not critical for the outcome of the simulations as long as $\epsilon_e \sim 1$; we have used $\epsilon_e = 1$ in this work). Such fast star formation is assumed to be triggered when the gas density of an SPH particle exceeds a certain critical value, chosen to be $n_{\rm H,e} = 0.3$ cm^{-3}; we have experimented with other values and found that the outcome of the simulations is very robust to changes in this parameter. In a star formation event an SPH particle is converted fully into a collisionless star particle of the same mass, thereby conserving the total number of particles in the simulation. The star particle remains a star for the rest of the simulation — non-instantaneous recycling is being implemented in a forthcoming version of the code. The moment of conversion from SPH to star particle is, as is customary, determined by a probabilistic approach.

The triggering of an SPH particle for star formation may (A) or may not (B) trigger a burst of self-propagating star formation (SPSF) in the cold, dense gas surrounding it: in scenario "A" not only the SPH particle which gets above the critical density threshold, but also its neighbouring cold and dense SPH particles with densities above $n_{\rm H,e,low}(< n_{\rm H,e})$ are triggered for conversion into star particles on their individual, dynamical timescales. Such self-propagating star formation is observed at present in some star-burst galaxies (e.g., in expanding super-shells — see Mori et al. 1997). SPSF is likely to have been more common at early times (when metallicities were lower and the ISM more homogeneous) — see McCray & Kafatos (1987). We stress that the above implementation of SPSF is just a simple, schematic way of modelling complicated (sub-resolution) physical processes.

For scenario "A" we ran 4 series of simulations with $n_{\rm H,e,low}$= 0.05, 0.1, 0.2 and 0.25 cm^{-3} respectively, corresponding to the conversion of approximately 5, 4, 3 and 2% of the gas mass initially in the simulation into stars at $z \gtrsim 5-6$; we dub this the "population III" scenario. The 4 different values of $n_{\rm H,e,low}$ were used to control the strength of the star-bursts to check whether the outcome of the simulations was sensitive to the choice of this parameter. In particular we wanted to check whether considerable fine-tuning is required to solve the AM problem. Early star-bursts converting more than about 5% of the initial gas into stars lead to halo star metallicities which are too large compared to observations (see section 5.2 and also SLGV99), so this sets an upper limit to the strength of the early star-bursts.

In scenario "B" only the initial SPH particle above the critical density threshold is triggered for star formation

on the dynamical time scale — we dub this the "population II" scenario.

When a star particle is formed, it is assumed to represent a population of stars born at the same time in accordance with a Salpeter IMF. It will hence feed energy back to the local ISM: during the first 5 Myr only stellar winds are assumed to contribute, during the subsequent about 35 Myr also (and more importantly) type II supernova explosions as well (the lightest stars which explode as SNII have a mass of about 8 $M_\odot$ and a lifetime of about 40 Myr). Only stars with masses greater than 30 $M_\odot$ are assumed to contribute significant amounts of energy to the ISM through winds, and such stars are assumed to deposit a total of 10^{50} ergs per star over their lifetime. Stars with masses greater than 8 $M_\odot$ are assumed to deposit 10^{51} ergs per star to the ISM as they explode as SNII at the end of their lifetime. The energy from the "star-burst" is deposited in the ISM as thermal energy at a constant rate over the lifetime of the burst, which is taken to be the above mentioned about 40 Myr (Mori et al. 1997). The burst energy is fed back to the, at any given time (<40 Myr), 50 nearest SPH particles using the smoothing kernel of Monaghan & Lattanzio (1985). Part of the thermal energy is subsequently converted into kinetic energy (by the code) as the resulting "super-shell" expands. While a star particle is feeding energy back to its neighbouring SPH particles, radiative cooling of these is switched off - this is an effective way of modelling with SPH a two-phase ISM consisting of a hot component ($T \sim 10^6 - 10^7$ K) and a much cooler component ($T \sim 10^4$ K) — see Mori et al. (1997); Gerritsen (1997) and Thacker & Couchman (2000, 2001). Scenario "A" above typically leads to complete "blow-away" of the remaining gas in the proto-galactic "dwarf" galaxy hosting the star-burst, whereas scenario "B" is much more gentle, but still leads to a considerable lowering of the density of the remaining gas.

- "Late" star formation mode

The gas which forms the disks of disk galaxies through smooth, dilute and fairly well ordered cooling flows has typically been heated to temperatures well above T_{crit} and has subsequently cooled down and settled onto the disk to become potentially star forming. Such gas is assumed to form stars on a much slower timescale

$$t_{*,l} = \frac{t_{dyn}}{\epsilon_l} \quad , \tag{2}$$

where $\epsilon_l \ll 1$. As discussed previously, such a large change of SFE between early and late phases of galaxy formation is in our experience required to form disks with the densities, radial and vertical structures, cold gas fractions, sizes and morphologies of observed disk galaxies at present. A value of ϵ_l=0.0025 was adopted in order to obtain (cold) gas fractions in the disk galaxies at $z = 0$ consistent with observational estimates (e.g., Sommer-Larsen 1996: the gas fraction (by mass) in Sa-Sc galaxies is ∼0.10-0.25 — the mean of our 28 SPSF disk galaxy runs (see section 4) is 0.17±0.01%, the dispersion 0.07). This adopted value of ϵ_l is somewhat low; we expect it to increase when non-instantaneous recycling of gas is properly taken into account in the simulations. Star formation through this "channel" is assumed to take place down to a quite low density threshold of 0.01 cm^{-3}. This, however, is still large enough to ensure that the gas has cooled down to a temperature $T{\sim}10^4$ K, at which the radiative cooling function is effectively truncated. For the (typically disk forming) star particles formed through this slow mode feedback was completely switched off. This is a crude, but effective way of modelling in our simulations the results of Mac Low & Ferrara (1999) obtained at much higher resolution, that for star-bursts in a well-organized, cold gas *disk* only a small fraction of the feedback energy is deposited in surrounding cold gas.

Finally we note that eq. (2) implies a star formation law in the continuous limit (and above the density threshold) of the form $\dot{\rho}_* \propto \rho_{\rm cg}^{1.5}$, where $\rho_{\rm cg}$ is the cold ($T{\sim}10^4$ K) gas density. The exponent of 1.5 is both physically and empirically (at $z{\simeq}0$) well motivated (Kennicutt 1998).

3. THE CODE AND THE INITIAL CONDITIONS

3.1. *The code*

We use the gridless Lagrangian N-body and Smoothed Particle Hydrodynamics code TreeSPH described in SLGV99. Our TreeSPH code is modelled after that of Hernquist & Katz (1989). The spline smoothing kernel of Monaghan & Lattanzio (1985) is used throughout for smoothing of gas dynamical properties as well as softening of gravity, as in Hernquist & Katz (1989). Individual time-stepping, implemented in a way similar to that of Springel, Yoshida & White (2001), is used in the code. The system time-step is always the smallest of all individual time-steps.

We include radiative gas cooling and heating in the simulations. The radiative heating corresponds to a redshift dependent, homogeneous and isotropic UV background radiation field produced by AGNs and young galaxies. This meta-galactic UV field is modelled after Haardt & Madau (1996) — the UV field switches on at redshift $z \sim 6$. The radiative cooling function is that of a primordial gas, modified by the effects of the UV field as discussed by, e.g., Vedel et al. (1994). The code furthermore incorporates inverse Compton cooling, which is also explicitly redshift-dependent. Star formation is incorporated by converting SPH particles into star particles by the schemes described in the previous section. The sum of the numbers of SPH and star particles is kept constant.

The smoothing length of each SPH particle is adjusted so as to keep the number of neighbors close to 50.

Finally, we have in this work used the shear-free Balsara (1995) viscosity, rather than the standard Monaghan-Gingold (1983) viscosity used previously.

3.2. *The initial conditions*

Our cosmological initial conditions are based on a ΛCDM model with $(\Omega_M,\Omega_\Lambda)$=(0.3,0.7) and a Hubble parameter $H_0 = 100h\,{\rm km\,s^{-1}\,Mpc^{-1}} = 65\,{\rm km\,s^{-1}\,Mpc^{-1}}$, resulting in a present age of the Universe of 14.5 Gyr. Following Eke, Cole, & Frenk (1996) we normalize the spectrum to $\sigma_8(z=0) = 1.0$, where as customary σ_8^2 is the mass variance within spheres of comoving radius $8h^{-1}$ Mpc, extrapolated from the linear regime of perturbation growth.

First, a cosmological N-body simulation (dark matter only) with 128^3 particles, a comoving box length of

10 h^{-1}Mpc and starting at a redshift of z_i=39 was run using the Hydra code (Couchman et al. 1995). At z=0, gravitationally bound dark matter haloes were identified by running a friends-of-friends algorithm with linking length 0.2.

Second, 12 dark matter haloes (see section 4) selected for detailed galaxy formation simulations were resampled and resimulated: For each dark matter halo a galaxy forming sub-volumne was determined by tracing all dark matter particles, which at z=0 were inside of 4 r_{200} (r_{200} being the radius inside of which the mean dark matter density is 200 times the critical), back to the initial conditions at z_i=39. The initial, co-moving linear extent of the galaxy forming sub-volume was ∼1.5-3 h^{-1}Mpc. At z_i, SPH particles were added to the galaxy forming sub-volume, one SPH per dark matter (DM) particle, with a mass of f_b times the original DM particle mass, where f_b is the baryonic fraction (see below). The masses of the DM particles in the sub-volume were reduced accordingly to $(1 - f_b)$ times the original mass. In the surrounding region of the cosmological simulation (with co-moving linear extent of about 10 h^{-1}Mpc) no SPH particles were added and the dark matter particles were increasingly coarsely resampled with increasing distance from the galaxy forming sub-volume. This, by now customary, procedure has been described by many authors, e.g., Navarro & White (1994); Gelato & Sommer-Larsen (1999) and Thacker & Couchman (2000). The galaxies were selected to be at least 1 Mpc away from galaxy groups and 0.5 Mpc away from larger galaxies at z=0. They were also selected such as not to undergo major merging events (with companion to parent mass ratios of 1:3 or more) since z=1.

We use a baryonic mass fraction $f_b = 0.10$, consistent with nucleosynthesis constraints ($0.015h^{-2} \lesssim \Omega_b \lesssim 0.02h^{-2}$) and with the observationally determined baryonic fractions in galaxy groups and clusters (e.g., Ettori & Fabian 1999). The masses of the SPH (and star) particles and the high resolution DM particles in the galaxy forming sub-volume are 4.0×10^6 and 3.6×10^7 $h^{-1}M_\odot$, respectively. The SPH particles are assigned an initial thermal energy corresponding to a temperature $T_i \simeq$ 100 K. Gravitational interactions between particles are softened according to the prescription of Hernquist & Katz (1989), with softening lengths of $\tilde{\epsilon}_{g,*}$=1.3 h^{-1}kpc for the gas and star particles and $\tilde{\epsilon}_{DM}$= 2.8 h^{-1}kpc for the high resolution DM particles. The gravitational softening lengths were kept fixed in co-moving coordinates until z=2.9, then constant in physical coordinates.

To check for effects of numerical resolution, one series of disk galaxy simulations was run with half these softening lengths, and one additional simulation was run with one quarter of these softening lengths and eight times higher mass resolution. For these latter simulations the softening lengths were kept fixed in co-moving coordinates until z=6.7, then constant in physical coordinates.

4. THE SIMULATIONS

We selected 12 dark matter haloes from the cosmological N-body simulation for the detailed galaxy formation runs. The masses of these haloes span about a factor of 10, with 4000–45000 dark matter particles inside r_{200} at z=0 and circular velocities at r_{200} ranging from about 100 to 185 km/s. After resampling the galaxy formation simulations consisted of 30000-150000 SPH+DM particles. We started out by running all 12 galaxy simulations using the self-propagating star formation prescription (mode "A" in section 2) with a lower density threshold of $n_{H,e,low}$=0.1 cm^{-3} (and $n_{H,e}$=0.3 cm^{-3}, as always). Seven of the resulting galaxies had at z=0 distinctly disk galaxy like morphologies and kinematics, the remaining 5 were lenticular (S0) or elliptical like. Four additional series of simulations were subsequently run for the 7 disk galaxies: three using again early SPSF with $n_{H,e,low}$=0.05, 0.2 and 0.25 cm^{-3} and one series with fast, early, but non self-propagating star formation (mode "B" in section 2). Typically, ∼30000 system time-steps were required to run from z_i=39 to z=0. To test for possible numerical effects we ran one additional (and more time consuming) series of 7 disk galaxy simulations with $n_{H,e,low}$=0.2 cm^{-3}, but with gravitational softening lengths of 0.65 h^{-1}kpc and 1.4 h^{-1}kpc for the SPH (and star) and dark matter particles, respectively — the outcome of these simulations compared fairly well with the results of the same simulations with "standard" gravitational softening lengths. We shall briefly discuss this in section 5.9. About 50000 system time-steps were required to run to z=0 for these simulations.

In addition we re-simulated one of the disk galaxies at an 8 times higher mass resolution (a very CPU intensive run). This was achieved by extracting the same region from cosmological initial conditions with identical parameters, but on a 256^3 mesh rather than the 128^3 grid used so far. Identical low-wavenumber Fourier modes were used for both grids, up to the Nyquist wavenumber of the coarser mesh. Above that, additional high-wavenumber modes were added to the finer mesh (up to its Nyquist wavenumber) to account for the extra small scale power in this simulation.

This procedure resulted in SPH (and star) and high resolution DM particle masses of 4.9×10^5 and 4.4×10^6 $h^{-1}M_\odot$, respectively. Moreover, we used a four times higher force resolution for this simulation corresponding to gravitational softening lengths of 0.33 and 0.69 h^{-1}kpc for the SPH (and star) and high resolution DM particles, respectively. The simulation was an SPSF run with $n_{H,e,low}$=0.25 cm^{-3} and the result is compared to that of the "standard" resolution simulation of the same galaxy (also with $n_{H,e,low}$=0.25 cm^{-3}) in section 5.9. This run required ∼80000 system time-steps.

Finally, to illustrate the importance of having a large initial SFE we ran the 7 "normal resolution" disk galaxy simulations with a constant, low SFE of ϵ=0.02. They were of the non SPSF type and run with the standard gravitational softening lengths.

In total we ran 12+4×7=40 "standard" galaxy formation simulations, 7+1 additional at higher resolution and 7 with a constant, low SFE. The computational costs amounted to about 5 years worth of single processor CPU time on a SGI Origin 2000 computer.

5. RESULTS

All results presented correspond to the final state of the simulations at redshift $z = 0$ unless otherwise explicitly mentioned. A general presentation of the results of the simulations at higher redshift will be given in a forthcoming paper.

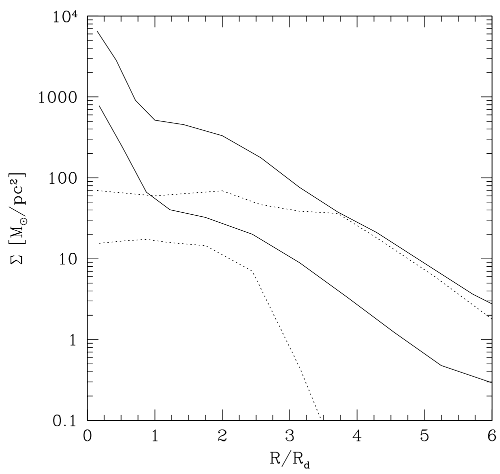

FIG. 1.— Surface density profiles for two Milky Way like disk galaxies, denoted S1 and S2 in this paper. Radial coordinate is in units of the exponential disk scalelength at z=0. Top curves correspond to S1; stars are marked by solid line, cold gas ($T\sim10^4$ K) by dotted. We estimate the (stellar) bulge-to-disk ratio of this galaxy to B/D=0.17±0.05. Bottom curves correspond to S2 — the curves have been displaced 1 dex downward for clarity (line-types as for S1). S2 has B/D=0.27±0.08.

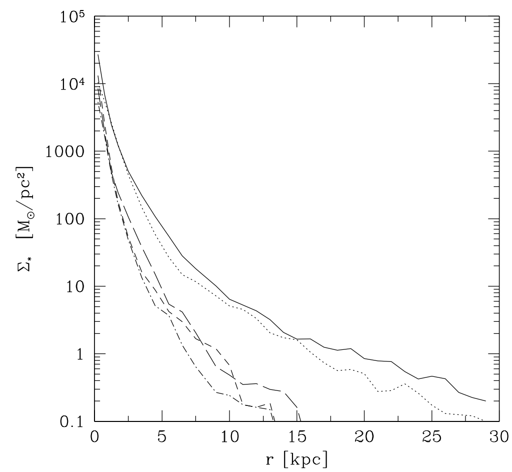

FIG. 2.— Stellar surface density profiles of the three elliptical and two lenticular galaxies.

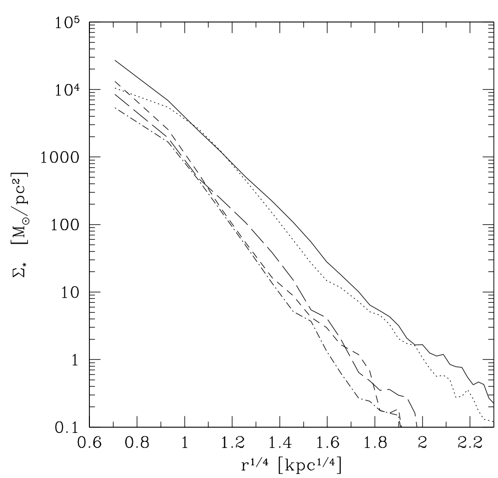

FIG. 3.— Same as in Fig. 2, but versus $r^{1/4}$.

5.1. *Surface density profiles, specific angular momenta and structural parameters*

As mentioned in the previous section, 7 of the 12 galaxies simulated have disk galaxy like morphologies and kinematics, with the bulk of the stars on approximately circular orbits in a disk, most of the rest of the stars in an inner, bulge-like component and finally a small fraction in a round and dynamically insignificant stellar halo surrounding the galaxies. The disk galaxies formed in our simulations are hence qualitatively quite similar to observed disk galaxies like the Milky Way. Of the remaining 5 galaxies, two have a minor fraction of the stars on nearly circular, disk orbits; we classify these as lenticulars (S0s) and the remaining three galaxies have no disks at all; we classify these as ellipticals — see further below.

The disk galaxies have approximately exponential stellar disk surface density profiles and exponential to $r^{1/4}$ bulge profiles, all in good agreement with observations. Two examples of a disk galaxy stellar surface density profile are shown in Figure 1 (for all stars within 2 kpc vertical distance from the disk) - the surface density of cold gas ($T \sim 10^4$ K) is also shown. The stellar profiles of the lenticular and elliptical galaxies are not exponential, as shown in Figure 2, but approximately follow an $r^{1/4}$ law, as shown in Figure 3.

The bulges of the disk galaxies are generally confined to being within a radius $r_B \sim 1-1.5$ kpc from the centers. Stellar disk scale lengths were determined by fitting exponential surface density profiles to the region of the disk outside of the bulge, $R > r_B$.

Bulge-to-disk ratios were determined by extrapolating the exponential disk profiles, obtained as described above, to the center of the galaxies. Using these decompositions (which make no assumptions about the bulge surface density profiles) the specific angular momenta of the stellar *disks* were estimated taking explicitly into account also the region with overlap between disk and bulge. As r_B is comparable to the gravitational softening lengths one has to check how affected the structural decomposition parameters are by gravity softening effects - we return to this at the end of the subsection.

Characteristic circular speeds V_c for the disk galaxies were calculated using the approach of SLD01, but as an addition taking into account also the dynamical effect of the bulges.

In Figure 4 we show the "normalized" specific angular momenta $\tilde{j}_* = j_*/V_c^2$ of the final disks formed in all 35 disk galaxy simulations as a function of V_c. As argued by SLGV99 one expects $\tilde{j}_*$ to be almost independent of V_c on both theoretical and observational grounds. Also shown in the figure is the median "observed" value of $\tilde{j}_*$, calculated as in SLGV99 and SLD01 for a Hubble

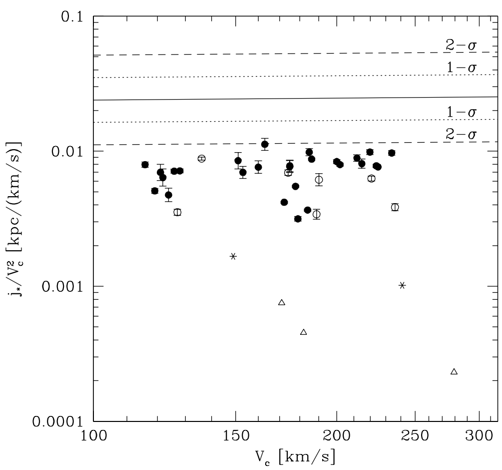

FIG. 4.— Normalized stellar specific angular momenta at z=0, $\tilde{j}_* = j_*/V_c^2$, of the galaxies formed in the simulations: Disk galaxies formed in the 4 series of runs with early, self-propagating star formation (SPSF) are shown by filled circles. The lenticulars (S0) and ellipticals (formed in the SPSF simulations with $n_{\rm H,e,low}$=0.10 cm^{-3}) are shown by star symbols and open triangles, respectively. Disk galaxies formed in simulations without self-propagating star formation are shown by open circles. The solid line shows the median value from the observational data on disk galaxies of Byun (1992), obtained as explained in SLD01 (but in this paper assuming H_0=65 km/s/Mpc), the dotted and dashed lines bracket the 1-σ and 2-σ intervals around the median.

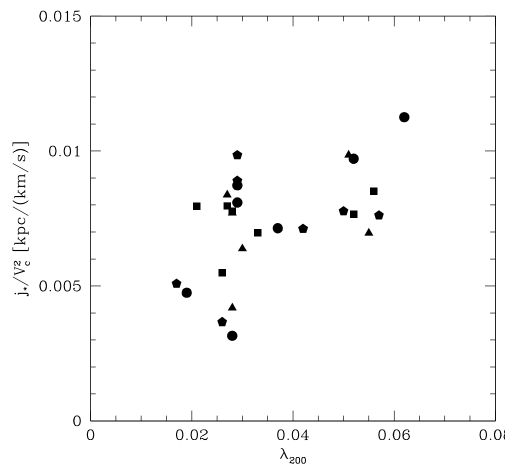

FIG. 5.— Normalized disk stellar specific angular momenta versus the spin parameter λ_{200} (evaluated at r_{200} of the dark matter halo) for the simulations with self-propagating star formation (SPSF). Filled triangles, squares, pentagons and circles correspond to $n_{H,e,low}$ = 0.05, 0.10, 0.20 and 0.25 cm^{-3}, respectively.

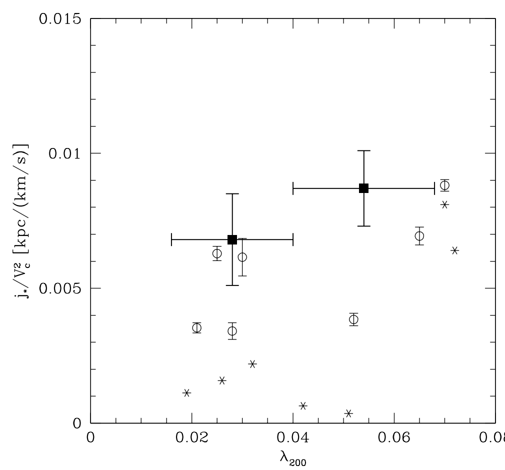

FIG. 6.— As Fig. 5, but for the disk galaxies formed in the 7 simulations without SPSF (shown by the open circles). Also shown (by filled squares) are the data for the 28 disk galaxies from Fig. 5 binned into two bins. The vertical bars on these last two data points are the dispersions in the two bins; the horizontal show the bin size. Finally, shown by star symbols are the results of the 7 constant, low SFE (ϵ=0.02) disk galaxy runs - no B/D decomposition was attempted for these galaxies, because they in general are very small and concentrated.

parameter of 65 km/s/Mpc, together with the observational 1-σ and 2-σ limits. As can be seen from the figure, the specific angular momenta of the stellar disks lie only about a factor of three below the observed median. This is about an order of magnitude better than what is obtained in similar CDM simulations not invoking stellar feedback processes, as discussed by many authors (e.g., Navarro, Frenk, & White 1995; SLGV99).

Also shown in the figure are the normalized specific angular momenta of the two lenticular and three elliptical galaxies. The "effective" V_c for these has been calculated using the stellar mass versus V_c relation for the disk galaxies (Figure 14). The specific angular momenta of the E/S0s are about an order of magnitude smaller than those of the disk galaxies, broadly consistent with observations (e.g., Navarro & Steinmetz 1997).

For the remainder of this paper we shall be concerned with the properties of the disk galaxies. We will analyze the E/S0s in detail in a forthcoming paper.

In Figure 5 we show the normalized specific angular momenta of the 28 disk galaxies from the SPSF simulations versus the dimensionless spin-parameter λ_{200} of their dark matter haloes ($\lambda \equiv J|E|^{1/2}/GM^{5/2}$ is evaluated at r_{200}). Fall & Efstathiou (1980) proposed that the angular momentum of a disk galaxy should be proportional to the spin-parameter of its dark matter halo, and indeed a positive correlation is seen in Figure 5, although the scatter is considerable (the linear correlation coefficient is 0.51, so the probability that $\tilde{j}_*$ and λ_{200} are uncorrelated is less than 3%). Filled triangles, squares, pentagons and circles correspond to $n_{H,e,low} = 0.05, 0.10,$ 0.20 and 0.25 cm^{-3}, respectively. It is clear from the figure that there is no statistically significant evidence that one particular choice of the parameter $n_{H,e,low}$ leads to a better solution of the AM problem than the other. Hence, for these SPSF simulations extreme fine-tuning of the amount of energetic feedback seems not to be required.

In Figure 6 we show the normalized specific angular momenta of the 7 disk galaxies from the simulations without SPSF versus λ_{200}. Also shown are the results

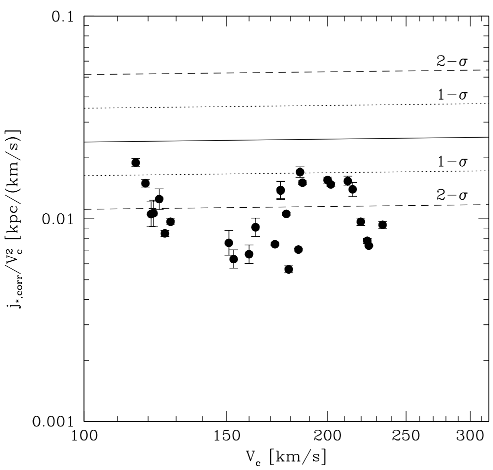

FIG. 7.— Spin-parameter corrected normalized specific angular momenta for the 28 disk galaxies formed in the simulations with SPSF. Line symbols as in Fig. 4.

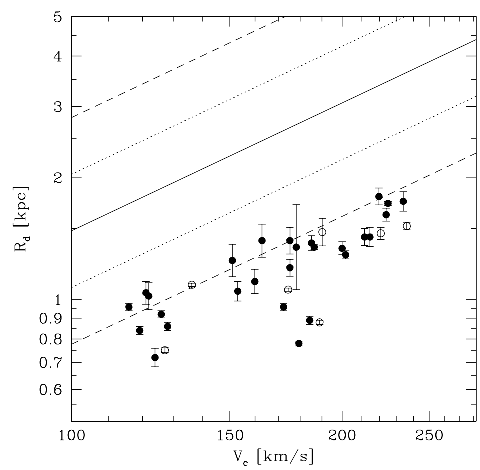

FIG. 8.— Exponential scale-lengths of all 35 disk galaxies (symbols as in Fig. 4). Line symbols as in Fig. 4.

from Fig. 5 binned into two bins. There is clearly an indication that the simulations without SPSF are not doing as well in terms of solving AM problem. We also show the results of the 7 constant, low SFE (ϵ=0.02) disk galaxy runs - these are in general giving very poor results in terms of solving the AM problem: the mean, spin-parameter corrected (see below), normalized angular momentum of these 7 runs is just 27±6% of that of the 28 SPSF runs.

The spin-parameters of our 7 disk galaxy haloes are on average somewhat smaller than the median found in cosmological N-body simulations — see below. This is most likely just an effect of small number statistics. Assuming (simplisticly) a linear relationship between $\tilde{j}_*$ and λ_{200} on the basis of the trend seen in Fig. 5 we correct the normalized specific angular momenta of the 28 disk galaxies formed in the SPSF simulations as follows to see how well we can expect to do in solving the AM problem. We assume a theoretical median value of λ of 0.05 (Barnes & Efstathiou 1987; Heavens & Peacock 1988) and hence multiply the normalized specific angular momenta of 28 disk galaxies by $(0.05/\lambda_{200})$. The results are shown in Figure 7. It is seen that the disk galaxies formed in SPSF simulations are really only deficient in specific angular momentum by about a factor of two relative to the observed median. The feedback+CDM scenario presented in this paper is hence doing almost as well as the WDM scenario discussed by SLD01 in terms of solving the AM problem for disk galaxies.

Although we are making an appropriate comparison between "observational" *disk* specific angular momenta and model *disk* specific angular momenta (both obtained through B/D decomposition) we note that some authors present total (disk+bulge) specific angular momenta for simulated galaxies. For comparison with these works we calculated $j_{*,tot}$ for the 35 model disk galaxies and found $< j_{*,tot} >= 0.87 < j_* >$, so the difference between the two types of specific angular momenta is quite small.

In Figure 8 we show the exponential scale-lengths of

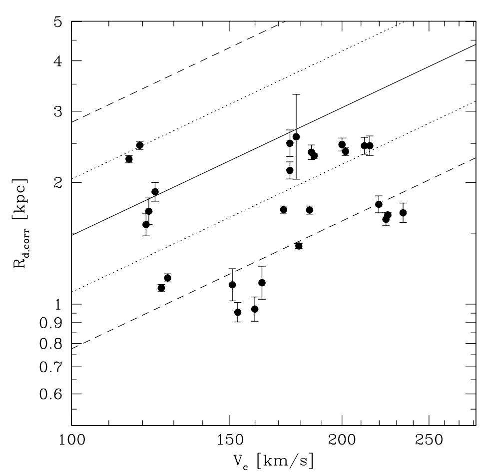

FIG. 9.— Spin-parameter corrected exponential scale-lengths of the 28 disk galaxies formed in the runs with early, self-propagating star formation — see text for details. Line symbols as in Fig. 4.

the 35 disk galaxies versus V_c. Not surprisingly, these are also too short by about a factor of two relative to the observed median (taken from SLGV99, but corrected to h=0.65). In Figure 9 we show the same, but corrected for spin-parameter effects, as discussed above, and only for the SPSF simulations, given the result shown in Figure 6.

In order to compare our model disk galaxies to observations some indicator of Hubble type T is required (as usual T=1 corresponds to Sa, T=2 to Sab, T=3 to Sb and so on). A seemingly obvious choice is the bulge-to-disk ratio B/D given the well-known correlation between the B–band bulge-to-disk ratio $(B/D)_B$ and galaxy type. What we have available from the decomposition of the model galaxies are *mass* B/D. Byun (1992) 2-D decomposed I-band images of ~ 1000 Sb-Sd galaxies ($3\leq T \leq 7$) from the sample of Mathewson et al. (1992). Contrary to

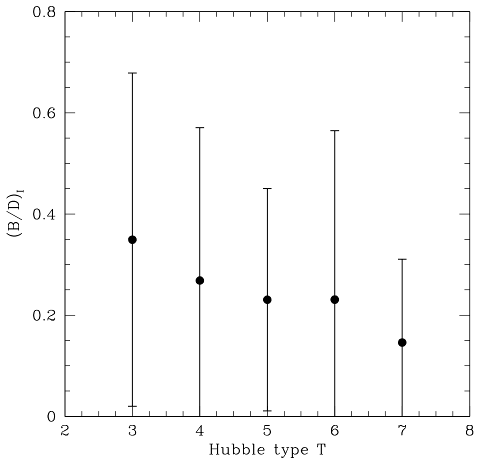

FIG. 10.— Mean I-band bulge-to-disk ratios versus Hubble Type T for the $\sim$ 1000 Sb-Sd galaxies for which Byun (1992) performed 2-D B/D decomposition. The bars correspond to the dispersion in each bin.

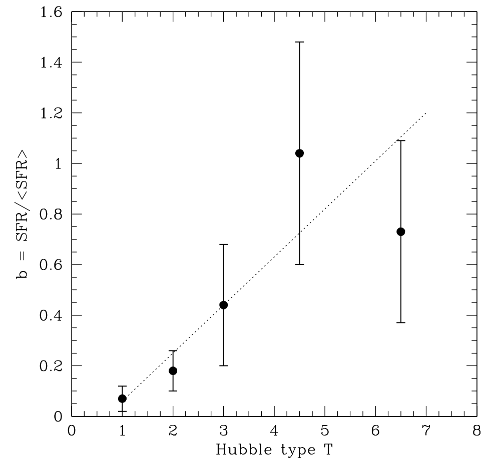

FIG. 11.— Mean birthrate parameter b versus Hubble Type T. The original data have been taken from Kennicutt et al. (1994) and the data shown have been 3-σ "clipped". The bars correspond to the dispersion in each bin and the dotted line is the linear fit to the data used in this paper (eq. 3).

$(B/D)_B$, I-band B/D trace the mass B/D better (e.g., Byun 1992). In Figure 10 we show the mean $(B/D)_I$ for the $\sim$ 1000 disk galaxies in Byun's sample. The bars correspond to the dispersion in $(B/D)_I$ for each Hubble type. Clearly, it is virtually impossible to classify a disk galaxy on the basis of its I-band (and hence approximately *mass*) B/D (at least for $3 \leq T \leq 7$).

Another potential disk galaxy type diagnostic is the so-called birthrate parameter, b, defined as the ratio of the present to past average star formation rate, $b = SFR/<SFR>$, for the *disk* stars — see Kennicutt, Tamblyn & Congdon (1994) and references therein. In Figure 11 we show the mean b versus Hubble type (T=1–7) for the data given in Kennicutt et al. (1994) after 3-σ "clipping". The bars correspond to the dispersion in b for each Hubble type. Clearly, b is a much better diagnostic of Hubble type than the mass B/D. A linear fit to the data yields

$$b = 0.19\,T - 0.13 \quad (1 < T \lesssim 5) \quad , \tag{3}$$

which is the relation we will use in the following when comparing our model disk galaxies to observations.

Figure 12 shows the stellar *mass* bulge-to-disk ratios B/D of the 35 disk galaxies versus the birthrate parameter b. As can be seen from Fig. 11 $b \sim 0.1$ for Sa's increasing to $b \sim 1$ for Sc's. The lack of trend seen in Fig. 12 is consistent with the weak trend found observationally for $(B/D)_I$ (and also for K-band B/D ratios, e.g., de Jong 1996), when allowing for the large dispersion in each bin seen in Fig. 10.

As mentioned previously, since r_B is comparable to the gravitational softening lengths, the structural bulge/disk decompositions can be affected by spurious effects of gravity softening (e.g., Bate & Burkert 1997; Sommer-Larsen, Vedel & Hellsten 1998a,b). To test for such effects we performed the following experiments: Switching star formation off and slowly reducing the softening lengths to final values half of the initial (which were 1.3 h^{-1}kpc for the gas (and star) particles and 2.8 h^{-1}kpc for DM particles), we continued the 7 disk galaxy SPSF runs with $n_{H,e,low} = 0.20$ cm^{-3} for one additional Gyr, starting at z=0. As the orbital time scale in the bulge and the main disk is considerably less than 1 Gyr the angular momentum distribution of the collisionless components (stars and dark matter) will be approximately preserved, as angular momenta are adiabatic invariants.

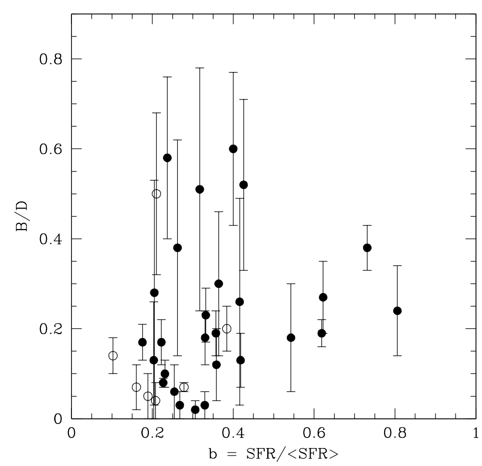

FIG. 12.— Bulge-to-disk ratios of all 35 disk galaxies versus birthrate parameters — see text for details (symbols as in Fig. 4).

We then performed the bulge/disk decomposition of the resulting 7 disk galaxies as before and found that the mean B/D increased by 0.20±0.07 (up from 0.20 to 0.40), the mean R_d by –0.07±0.16 kpc and the mean disk j_* by 38±73 kpc km/s (up from 229 to 267 kpc km/s) as the softening lengths were reduced by a factor of two. We do not expect any significant further changes

if the softening lengths were reduced even more since now $\tilde{\epsilon}_{g,*} < r_B$ and the central gravitational potential is completely dominated by stars and gas. So a statistically significant increase in the mean B/D ratio results from going to smaller softening lengths, bringing it in better agreement with the recent estimate of $\lesssim$0.6 for the *mass* B/D ratio independent of disk galaxy type (Portinari, Sommer-Larsen & Tantalo 2003). As a consequence the resulting *disk* j_* would be expected to increase somewhat. This is indeed hinted by the above results though the statistical significance of this can not be established on the basis of the present 7 experiments. The disk scale lengths appear to be only slightly overestimated (by 6±14%).

5.2. *Broad band B–V colours of the disk galaxies*

Besides the birthrate parameter, a variety of other characteristics of observed galaxies is known to depend on their Hubble type (see e.g. the review by Roberts & Haynes 1994). In this Section we discuss the integrated B–V colours of our simulated disk galaxies.

We estimate their colours "post-process": First we calculate the average chemical enrichment history of each galaxy on the basis of its star formation history (SFH), inferred from the age distribution of the stars in the final galaxy (inside of r=30 kpc) at $z = 0$. Once the metallicity evolution $Z(t)$ is computed, we derive from the star formation rate $\Psi(t)$ of the galaxy its integrated luminosity L in any given passband as:

$$L = \int_0^{t_G} \Psi(t)\, L_{SSP}(t_G - t, Z(t))\, dt \qquad (4)$$

where t_G is the age of the galaxy and $L_{SSP}(\tau, Z)$ is the luminosity of a Single Stellar Population (SSP; Tinsley 1980; Renzini & Buzzoni 1986) of age τ and metallicity Z. In the following we give further details on the individual ingredients in calculating the B–V colours.

5.2.1. *The chemical evolution history*

The metal enrichment is calculated post-process, with the purpose of obtaining an approximate estimate of the integrated B–V colours of the disk galaxies.

Some level of global pre-enrichment is expected from the initial "fast" star formation activity responsible for the early feedback effects (see Section 2). This early star formation is localized in the cool gas clouds but otherwise widely distributed over the simulation volume; it typically peaks at redshifts $z{\sim}6$–8 (for the SPSF runs — see Section 5.4), followed by a more gentle level of activity. A second phase of star formation, associated with the formation of the main galaxy itself, commences at redshifts $z \sim 4 - 5$. As a first approximation one can hence divide the star formation and chemical enrichment history into two phases: an early phase resulting in fairly uniform metal (pre)enrichment of the simulation volume and a second corresponding to the formation of the main galaxy.

The level of pre-enrichment is calculated with a chemical evolution model representing a closed-box with the same SFH as that of the entire simulation volume. We use the chemical evolution model by Portinari, Chiosi & Bressan (1998), suitably modified so as to treat the SFH $\Psi(t)$ as an input information, rather than calculating its own star formation rate after a prescribed Schmidt-like law. A Salpeter Initial Mass Function (IMF) is assumed throughout the calculations, with logarithmic slope 1.35 and mass limits 0.1—100 $M_\odot$. The metallicity of the closed-box at t =1.5 Gyr ($z = 4.2$) is taken as the level of pre-enrichment for the subsequent second phase of main galaxy formation. We obtain levels of pre-enrichment in the range 1/100 to 1/20 $Z_\odot$ (increasing as the strength of the early star-bursts increases, causing a larger fraction of gas to be converted into stars during this early phase — see Section 2), with 1/40 $Z_\odot$ as the typical value.

Starting from the appropriate initial metallicity level, we then calculate the chemical evolution of the main galaxy based on its SFH during the remaining 13 Gyr (from 1.5 to 14.5 Gyr). The SFH is directly provided by the age distribution of the star particles that reside in the galaxy at the end of the simulation. For the chemical evolution of the main galaxy, the closed-box assumption would be too crude an approximation: not all the baryons that end up in the final galaxy are immediately and equally available for star formation since the beginning, as the closed-box model would presume. Realistically, what happens is that gas progressively cools out and becomes available for star formation ($T \sim 10^4$ K, $n_H \gtrsim 0.01$ cm^{-3}). We can regard this "cool out" as a sort of "infall history" for the galaxy. We estimate the accretion history of cold gas onto the main galaxy as follows. At each time t, we know the total amount of cold gas in the simulation volume, $M_{cg}^{tot}(t)$, as well as the total star formation rate $\Psi^{tot}(t)$, and the SFH of the stars that end up in the galaxy, $\Psi(t)$. The rate at which cold, dense gas becomes available for the star formation relevant to the main galaxy, is simply approximated by:

$$M_{cg}(t) = M_{cg}^{tot}(t)\, \frac{\Psi(t)}{\Psi^{tot}(t)} \qquad (5)$$

Hence we calculate the chemical evolution of the galaxy assuming an infall model with a mass accretion history given by:

$$M(t) = M_{cg}(t) + M_*(t) \qquad (6)$$

where $M_*(t)$ is the mass of the stars in the final galaxy that were formed up to time t. To do so, we further adapted the chemical evolution model by Portinari et al. (1998) so that it could treat not only the SFH, but also the accretion history as input data, in place of the usual prescription $\dot{M} \propto e^{-\frac{t}{\tau}}$.

Post-process calculation of chemical evolution introduces some inconsistency with respect to the results of dynamical simulations, since the chemical model accounts for the gas re-ejection from dying stars, which is neglected in the simulations. Hence, for the same SFH the two models will end up with a somewhat different gas versus star content. For the Salpeter IMF adopted here, a SSP restitutes ∼30% of its mass to the gaseous phase over a Hubble time, hence this is the order of magnitude of the discrepancy between the final mass in stars in the chemical model and in the dynamical simulation. A consistent calculation of the metallicity distribution of the stars in the galaxy would require chemical evolution to be implemented in the simulations, so that each star particle is consistently labelled with its own age and metallicity and can be individually treated as a SSP for the sake of colour calculation. This is currently being

implemented in the code. The above mentioned mismatch in final mass in stars, however, mostly affects the integrated magnitude of a galaxy, while its colour is only marginally sensitive to the slightly different metal enrichment for different gas fractions. Hence, for the purpose of this paper our post-process estimate of the colours is adequate.

5.2.2. *The calculation of "integrated" B–V colours*

The chemical evolution calculated above provides us with the metal enrichment history $Z(t)$ of the galaxy, which combined with its known SFH $\Psi(t)$ allows us to calculate its integrated luminosity from Eq. (4). As to L_{SSP}, we adopt the magnitudes and colours of the SSPs by Tantalo et al. (1996).

The B–V colours, calculated as described above, do not include the effects of dust and gas re-processing of the stellar radiation, which can be crucial especially for the youngest stellar populations. In particular, there is evidence from studies of combined dust extinction and IR re-emission that the youngest stellar populations can be heavily obscured by the parent clouds for periods of up to a few 10^7yr (e.g. Silva et al. 1998; Charlot & Fall 2000). In the current paper we deal with this effect in the following simple way: We calculate the B–V colour for each galaxy by including all stars formed to the present (corresponding to no "dust correction" at all) and by dropping the light contribution of the stars formed in the last 2×10^7 yr; we consider the range of colours we obtain as our uncertainty and denote the mean of the two values $(B\text{–}V)_0$. As to the extinction from the diffuse gas phase, the reddening effect on B–V for spiral disks is mild (e.g. Boissier & Prantzos 1999) and moreover the observed colours from Roberts & Haynes which we use for comparison are the RC3 catalogue "intrinsic" $(B\text{–}V)_0$ colours, which have been corrected for internal extinction.

Further uncertainties and systematic effects on the colours may come from the choice of the IMF, which influences the level of chemical enrichment. Dynamical arguments favour a rather low M/L ratio in spiral galaxies, both for external galaxies and for our Milky Way (Sommer-Larsen & Dolgov 2001 and references therein — see also section 5.3), implying a more bottom-light IMF than the standard Salpeter one adopted here. A variety of studies in fact suggest the the slope of the IMF gets much shallower than the Salpeter value below 1 $M_\odot$ (e.g. Kroupa et al. 1993; Chabrier 2003). In the present paper, however, we consistently use a Salpeter IMF since our main purpose is to discuss the *trend* of the B–V colours with respect to other galactic properties, such as Hubble type etc.

Finally, systematic differences in the broad-band colours of SSPs among different authors exist, while better agreement is found for the differential variation of SSP colors with age and metallicity (e.g. Charlot, Worthey & Bressan 1996; Kodama & Arimoto 1998). So, given the above-mentioned sources of uncertainty (dust, IMF and theoretical SSPs) the *trend* of broad-band colours with the properties of simulated galaxies is to be considered more robust than their absolute values.

The B–V colours we obtain are compared to the observed ones from the review by Roberts & Haynes (1994), which is based on a large sample of galaxies compiled from the RC3 catalogue. We use the disk galaxy birthrate parameter b as our morphology indicator and convert from the observational morphological type T to b as described at the end of Section 5.1 (using eq. 3).

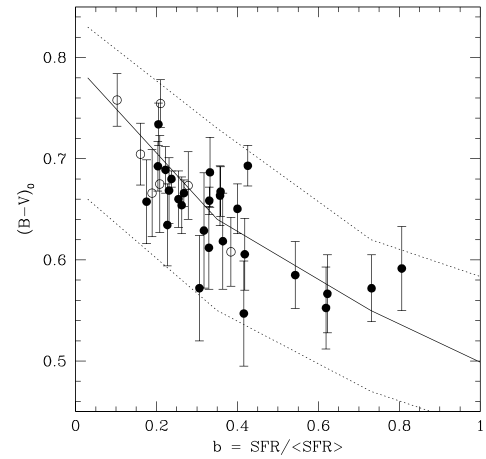

FIG. 13.— Integrated $(B\text{–}V)_0$ colours of all 35 disk galaxies, calculated using stellar population synthesis techniques — symbols as in Fig. 4. Also shown (solid line) are the mean observational values for disk galaxies from Roberts & Haynes (1994) and the observational 1-σ limits (dotted line).

In Figure 13 we show the predicted $(B\text{–}V)_0$ colour for the 35 disk galaxies versus the b parameter. Also shown are the observational results from Roberts & Haynes. The agreement between theory and observations is certainly satisfactory.

5.3. *The Tully-Fisher relation and mass-to-light ratios of disk galaxies*

In Figure 14 we show the stellar mass of the final disk galaxies formed in 35 runs versus the characteristic circular speed. Also shown is the I-band Tully-Fisher relation (TF) of Giovanelli et al. (1997a) for h=0.65, converted to mass assuming (stellar) mass-to-light ratios M/L_I = 0.5, 1.0 and 2.0 in solar units (used throughout) and applying an 0.2 mag. offset (Giovanelli et al. 1997b) to take into account that the typical disk galaxy in our sample is of type Sab. The slope of the "theoretical" TF matches that of the observed one very well for a constant mass-to-light ratio, which is required to be $(M/L_I) \sim 0.8$. This fairly small value required is consistent with the findings of SLD01 for their WDM simulations. Such a low value is fairly consistent with recent dynamically and/or lensing estimated mass-to-light ratios for disk galaxies (e.g., Vallejo, Braine & Baudry 2002; Trott & Webster 2002), the mass-to-light of the Milky Way (SLD01) and can be obtained from stellar population synthesis models provided an IMF somewhat more top-heavy (or more appropriately: more bottom-light) than the Salpeter law is used (Portinari, Sommer-Larsen & Tantalo 2003). The observed chemical enrichment of galaxy clusters and the global cosmic star formation and enrichment history seem to require an IMF with similar properties (Pagel 2002).

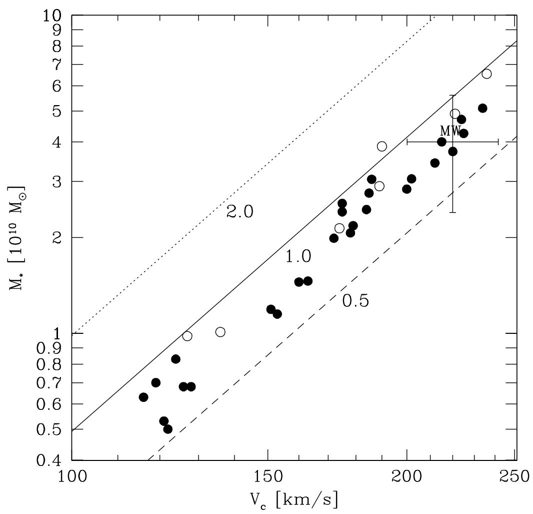

FIG. 14.— The stellar mass vs. circular velocity "Tully-Fisher" relation for the galaxies from the 35 simulations resulting in disk galaxies (symbols as in Fig. 4). Also shown is the observed I-band TF relation for Sc galaxies of Giovanelli et al. (1997) converted to mass assuming (M/L_I)=0.5 (*dashed line*), 1.0 (*solid line*) and 2.0 (*dotted line*) and applying an 0.2 mag. offset to correspond to Sab galaxies (Giovanelli et al. 1997b), which is the mean type of our simulated disk galaxies. Finally, the symbol "MW" with errorbars shows the likely range of the stellar mass and characteristic circular velocity of the Milky Way (from SLD01, but corrected to stellar mass, rather than total baryonic mass).

5.4. *Disk galaxy gas accretion rates*

We have calculated the rates at which hot halo gas cools out and subsequently is deposited onto the disks of the 35 disk galaxies in our sample. This is of considerable interest because observational upper limits can be placed on the accretion rate of gas onto the Galactic disk and potentially also other disk galaxies.

As hot halo gas (at $T_{\rm max} \sim 10^6$ K) starts to cool out near the disk and finally is deposited onto it, at some much lower temperature ($T_{\rm min} \sim 10^4$ K) highly, but not fully, ionized atoms like OVI will be present in the transition region. Denoting the accretion column density of H atoms per unit time by $\dot{N}_H$ and the initial (hot halo gas) H density n_{H0} and neglecting heat conduction, one can show that the column density of an ion Z^i produced between temperatures $T_{\rm min}$ and $T_{\rm max}$ is

$$N_Z^i = k\frac{\dot{N}_H}{n_{H0}} A_Z \int_{T_{\rm min}}^{T_{\rm max}} (\frac{3}{2}+s)\frac{\chi}{\chi_e}\frac{f_i dT}{(n_H/n_{H0})\Lambda} \quad , \qquad (7)$$

where k is the Boltzmann constant, A_Z is the abundance of the element relative to hydrogen, s is 1 for isobaric and 0 for isochoric cooling, χ is the number of particles per H atom, χ_e the number of electrons per H atom, f_i is the fraction of atoms of element Z which are in ionization stage Z^i, n_H is the H density of the cooling, transition-phase gas, and Λ is the cooling function, such that $\Lambda n_H n_e$, where n_e is the free electron number density, is the energy loss rate per volume (Edgar & Chevalier 1986, EC). For isobaric cooling (which, cf. EC, is the most relevant case for the present problem) EC find N(OVI)=$3.8{\cdot}10^{14}$ cm^{-2} for $\dot{N}_H/n_{H0}$=10^7 cm/s and assuming solar gas abundance and composition.

The result does not change much for hot halo gas oxygen abundances as low as 1/10 solar: Galactic halo stars are observed to be α-element enhanced, reflecting that the heavy elements in the stars were primarily produced by type II supernovae. For halo stars [O/H]=–1.0 corresponds to [Fe/H]$\simeq$–1.4 (e.g., Pagel 1997). One would expect that the hot halo gas is α-element enhanced as well, since the heavy elements in the gas most likely originate from a) the early phase of halo star formation and/or b) star-bursts in the Galactic disk. In the latter case the heavy elements produced by the type II supernovae are transported to the halo via fountain flows (e.g., Mac Low & Ferrara 1999). For [Fe/H]$\simeq$–1.4 the radiative (collisional ionization equilibrium) cooling function is almost an order of magnitude less than for [Fe/H]=0.0 (e.g., Sutherland & Dopita 1993). Hence it follows from eq. (7) that N(OVI) should be similar for 1/10 solar and solar gas oxygen abundance (for the same $\dot{N}_H/n_{H0}$). Even if the gas has solar iron-element abundance *and* is α-element enhanced with [O/Fe]$\simeq$0.4 due to SNII driven fountain outflows from the disk the estimate of N(OVI) (at a given $\dot{N}_H/n_{H0}$) should not increase by more than about 50% because of the increased (radiative) cooling efficiency resulting from the α-element enhancement.

From OVI absorption lines in the spectra of $\sim$ 100 AGNs observed with *FUSE (Far Ultraviolet Spectroscopic Explorer*), Blair Savage and collaborators find N(OVI) $\sin|b| \simeq 1.8{\cdot}10^{14}$ cm^{-2} and $\simeq 1.3{\cdot}10^{14}$ cm^{-2} in the Northern and Southern Galactic hemispheres, respectively (Savage et al. 2003). Assuming $n_{H0} \sim 10^{-3}$ cm^{-3} (EC; B. Savage, 2002, priv. comm.; also what is found from our simulations) and combining both sides of the disk, this yields a gas accretion rate of $2.9{\cdot}10^{-3}$ M$_\odot$/yr/kpc^2 locally ("locally" for the observed, OVI absorbing gas actually corresponds to a fairly large region of the disk out to about 5 kpc from the sun, B. Savage, 2002, priv. comm.). Assuming a characteristic size of the Milky Way's gas disk of R=15-20 kpc and that the above local accretion rate is typical, one obtains an estimated total accretion rate of about 2.0-3.6 M$_\odot$/yr with an uncertainty of at least a factor of two. Part (and perhaps most) of this is not likely to stem from hot halo gas cool-out, but from fountain flows (B. Savage, 2002, priv. comm.).

In Figure 15 we show the present day disk gas accretion rates of the 35 disk galaxies versus their characteristic circular speed. It is seen that disk galaxies with characteristic circular speed comparable to that of the Milky Way ($V_c \simeq 220$ km/s) are found to have accretion rates of about 0.5–1 M$_\odot$/yr at z=0, broadly consistent with the above observational upper limit.

As an alternative source of gas infall, in particular in relation to the "G-dwarf problem" (see section 5.6), the HI high-velocity clouds (HVC) have been considered. We note that the accretion rate predicted by our models is comparable to the maximum Tosi (1988) could obtain with HVCs under a number of favorable assumptions. With the "new" source of gas infall discussed in this paper (cooled-out halo gas) it is no longer required to appeal to HVC's as the primary source of gas infall onto the Galactic disk.

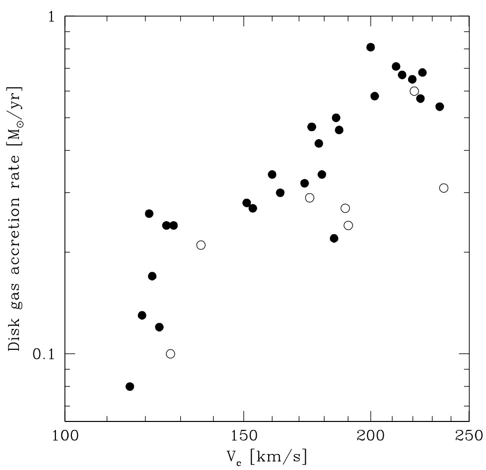

FIG. 15.— Disk gas accretion rates at z=0 for the 35 model disk galaxies (symbols as in Fig. 4).

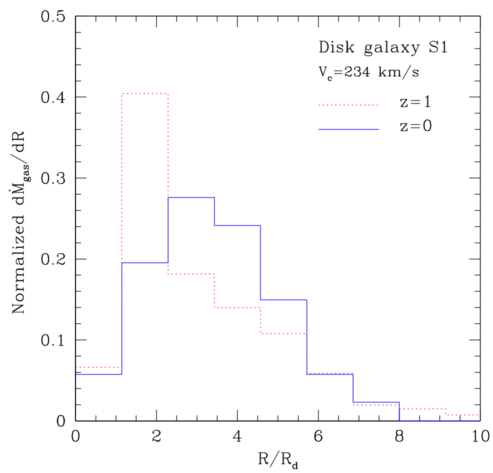

FIG. 16.— Normalized disk gas accretion rates per radial bin at z=1 and z=0 for model disk galaxy S1 — example of "inside-out" disk formation.

More generally, one can show that the rate at which hot gas cools out in the halo is proportional to $L_{\rm X,bol}< \frac{1}{T} >$, where $L_{\rm X,bol}$ is the bolometric X-ray luminosity and $< \frac{1}{T} >$ is the mean, emissivity weighted inverse temperature of the hot halo gas (Toft et al. 2002). Only few relevant X-ray observations of external disk galaxies are currently available, but forthcoming XMM-Newton and Chandra observations of nearby, nearly edge-on, isolated and undisturbed disk galaxies should greatly improve the situation and enable the determination of gas accretion rates for external disk galaxies from the bolometric X-ray luminosity of their hot haloes (Toft et al. 2002).

For the simulations presented in this paper we have assumed that the gas has primordial abundance. If the gas abundance is 1/3 solar, as in the intra-cluster medium, it follows from the work of Toft et al. that the bolometric X-ray luminosities and hence gas accretion rates will be a factor of 3-4 *lower* at z=0, so for a Milky Way like disk galaxy about 0.1–0.3 M$_\odot$/yr would be expected, even more consistent with the upper limit for the Galactic disk, deduced from OVI observations.

5.5. *Disk formation: "inside-out" versus "outside-in"*

It is frequently advocated that in hierarchical structure formation scenarios, such as the CDM scenario, the formation of galactic disks proceeds "inside-out" in the sense that an initial formation of the inner parts of the disk is followed by a phase of gradual increase of the size of the disk lasting for a Hubble time (e.g., White & Frenk 1991; Sommer-Larsen 1991; Mo, Mao & White 1998). With the models presented here we are in a position to test this "inside-out" paradigm. In two of the 12 dark matter haloes used in this work disk galaxies with circular speeds comparable to that of the Milky Way are formed. Of the total of eight SPSF simulations run with these two haloes, we analyze for the larger halo the one with $n_{H,e,low}$=0.25 cm^{-3} and for the smaller halo the one with $n_{H,e,low}$=0.20 cm^{-3} — the other SPSF simulations of these two haloes give similar results, but the runs selected are the ones which result in the largest j_*, being 19 and 11% larger than the mean for the four SPSF runs per halo, respectively. The disk galaxy formed in the largest of the two haloes has V_c=234 km/s and stellar and cold ($T \simeq 10^4$K) gas masses of M_*=5.2·10^{10}M$_\odot$ and $M_{\rm cg}$=0.9·10^{10}M$_\odot$, respectively — we shall denote this disk galaxy S1 in the following. The other disk galaxy formed in the smaller of the two haloes has V_c=212 km/s, M_*=3.5·10^{10}M$_\odot$ and $M_{\rm cg}$=0.6·10^{10}M$_\odot$ at z=0 — we denote it S2. These and other physical parameters for the two galaxies are given in Tables 1 and 2.

In Figure 16 we show the rate at which cooled-out gas is accreted onto the disk of S1 per radial bin at redshifts z=1 and z=0. The rate has been normalized to unity over the entire disk at each redshift and is shown versus the radial coordinate in the disk in units of the (stellar) disk scale length at z=0, R_d. This disk is overall clearly forming "inside-out", but we note that already at z=1 it is accreting gas out to $\sim$ 6–8R_d, and at z=0 gas is still accreting onto the inner parts of the disk. Figure 17 is similar to Fig. 16, just for galaxy S2. It is apparent from the figure that the formation of this disk occurs in a strikingly different, "outside-in" manner. At z=1 it is, like S1, already accreting gas out to $\sim$ 6–8R_d, but at z=0 the gas inflow has contracted to $R \lesssim 4R_d$. Hence, though one should obviously not draw any far reaching conclusions on the basis of just two Milky Way like model disk galaxies, out results indicate that disk formation (not surprisingly) is a more complicated process than depicted in the above mentioned analytical or semi-analytical works.

That gas is being deposited onto the disks out to $\sim$ 6–8R_d is also interesting in relation to the observational finding that present day HI disks often extend well beyond the (stellar) Holmberg radius $R_{26.5}$ ($\sim$ 4–5 R_d — see van der Kruit & Searle 1982), in fact to about 1.5$R_{26.5}$ (e.g., Wolfe et al. 1986). We shall in a forthcoming paper discuss the implications of our models in relation to observed medium to high-z damped Lyα systems (DLAs).

TABLE 1
MASSES[a] OF AND NUMBER OF PARTICLES[a] IN SELECTED DISK GALAXIES AT z=0

Galaxy	M_* [10^{10}M$_\odot$]	M_{cg} [b] [10^{10}M$_\odot$]	M_{hg} [c] [10^{10}M$_\odot$]	$M_{b,tot}$ [d] [10^{10}M$_\odot$]	N_*	N_{cg} [b]	N_{hg} [c]	$N_{b,tot}$ [d]
S1	5.16	0.91	0.03	6.10	8493	1495	54	10042
S2	3.46	0.61	0.03	4.10	5697	1001	56	6754
S3	1.48	0.46	0.03	1.97	2431	763	47	3241
S3-8	1.65	0.20	0.03	1.88	21713	2684	381	24778

[a] Within galactocentric distance r=30 kpc
[b] Gas with $T \leq 3 \cdot 10^4$ K
[c] Gas with $T > 3 \cdot 10^4$ K
[d] Total baryonic mass and number of particles

TABLE 2
OTHER PHYSICAL PROPERTIES OF SELECTED DISK GALAXIES AT z=0

Galaxy	V_c [km/s]	j_* [kpc km/s]	j_{cg} [kpc km/s]	B/D	R_d [kpc]	$\dot{M}_{gas}$ [M$_\odot$/yr]	SFR [M$_\odot$/yr]	b	Type
S1	234	532±21	1147	0.17±0.05	1.75±0.10	0.54	0.98	0.22	Sab
S2	212	400±23	387	0.27±0.08	1.43±0.07	0.71	1.70	0.62	Sbc
S3	163	236	664	0.28	1.28	0.30	0.22	0.19	Sab
S3-8	166	248±20	936	0.28±0.13	1.17±0.05	0.16	0.26	0.20	Sab

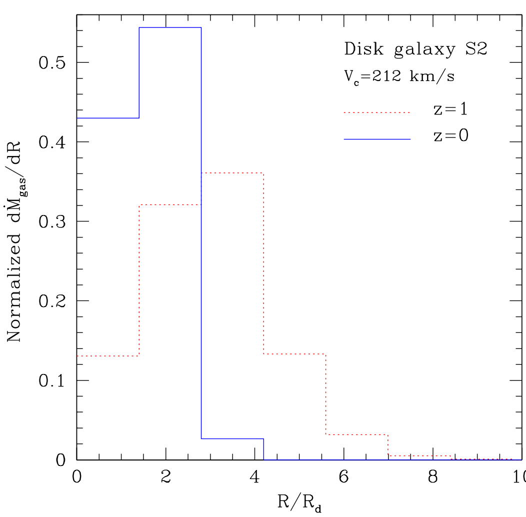

FIG. 17.— Normalized disk gas accretion rates per radial bin at z=1 and z=0 for model disk galaxy S2 — example of "outside-in" disk formation.

The total gas accretion rates for galaxies S1 and S2 (integrated over the entire disk) are 0.5 and 0.7 M$_\odot$/yr at z=0 and 3.0 and 4.5 M$_\odot$/yr at z=1, so the gas accretion rates are $\sim$ 6–7 times larger at z=1 than at z=0. The masses of S1 and S2 at z=1 are M_*=3.5 and 1.8 $\cdot 10^{10}$M$_\odot$ and $M_{\rm cg}$=1.7 and 0.9$\cdot 10^{10}$M$_\odot$, respectively. Given the considerable drop in gas accretion rates from z=1 to z=0, that the galaxies are accreting gas out to $\sim$ 6–8R_d at z=1 and the fairly modest increase in total mass from z=1 to z=0, it seems safe to conclude that the formation of isolated large disk galaxies was well under way by redshift $z \sim 1$. This seems in line with the observations by Simard et al. (1999), which indicate that disk galaxies have similar sizes at $z \simeq 1$ and z=0.

In Figure 18 we show for galaxies S1 and S2 the mean age of disk stars (within 2 kpc vertical distance from the disk) versus radial coordinate in units of the (stellar) disk scale length at z=0. The bars correspond to the dispersion in each bin. Only stars with formation redshift $z_f < 2.6$ (corresponding to ages $\lesssim$ 12 Gyr) were included — this eliminates essentially all halo stars and also partly the bulge stars for these two galaxies. In the disk of S1 there is essentially no age gradient and the mean stellar age is $\sim$ 7–8 Gyr corresponding to a mean formation redshift of $\sim$ 0.8 (in the two innermost bins the mean age is larger due to contribution from bulge stars). The disk age dispersion is $\sim$ 2-3 Gyr corresponding to a dispersion in redshift of $\sim$ 0.3-0.4. At first it seems surprising that a disk, forming inside-out, has no age gradient. However, firstly the star formation history is generally different from the gas accretion history, and secondly the star formation rate depends non-linearly on the cold gas density, $\dot{\rho}_* \propto \rho_{\rm cg}^{1.5}$ (cf. eq. 2). This makes the star formation rate quite low in the outer disk at late times and hence the average stellar age quite high there (but some young stars are present — see below).

The mean age of the stars in the outer disk of galaxy S2 is $\sim$ 6–7 Gyr — slightly less than the outer disk of S1. The mean age decreases with decreasing R to about 4 Gyr in the third innermost bin. This is not surprising given the gas accretion patterns at z=1 and z=0 shown in Fig. 17. In the two innermost bins there is some contribution from bulge stars (with $z_f < 2.6$) increasing the mean age there to 6-10 Gyr.

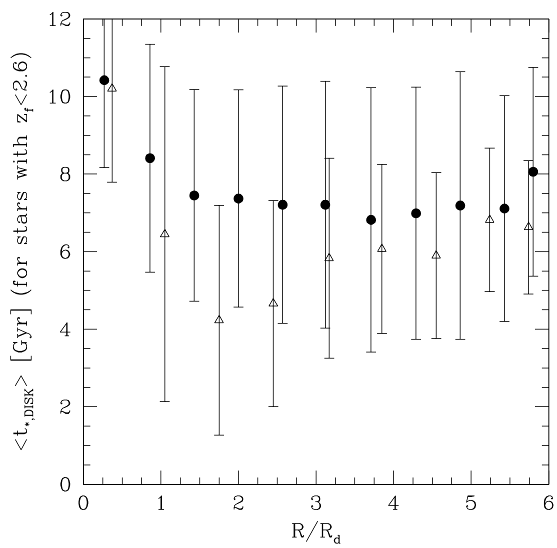

FIG. 18.— Mean ages of disk stars in galaxies S1 (solid circles) and S2 (open triangles). Only stars with formation redshift z_f <2.6 (or equivalently age $\lesssim$ 12 Gyr) are included. The bars show the age dispersions in each bin.

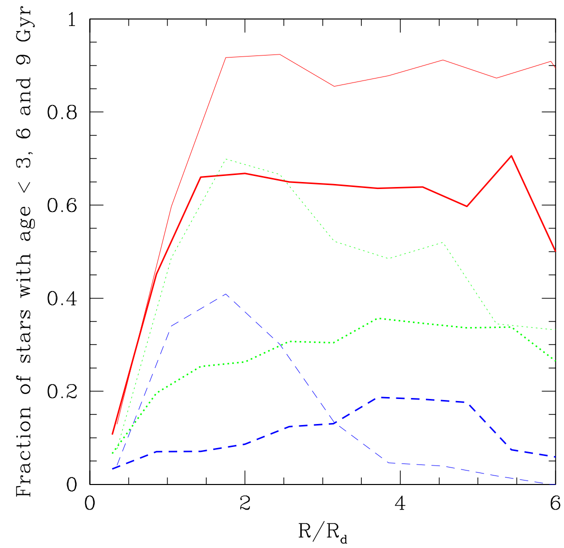

FIG. 19.— Distribution of stellar ages in the disks of galaxies S1 (thick curves) and S2 (thin curves) as a function of the radial coordinate in the disk. Only stars with z_f <2.6 (or equivalently age $\lesssim$ 12 Gyr) are considered. The fraction of these younger than 3, 6 and 9 Gyr are marked by dashed, dotted and solid lines, respectively. The inner $\sim 1.5 R_d$ are dominated by bulge stars.

To gain more insight than what can be obtained from mean ages, we show in Figure 19 the distributions of stellar ages as a function of the radial coordinate in the two disks (again for stars with $z_f < 2.6$). The fractions of stars younger than 3, 6 and 9 Gyr are shown for the disk of S1 with thick curves and for S2 with thin ones. For S1 the fractions of stars younger than 3 and 6 Gyr increase steadily with R out to $R \sim$ 4–5R_d. So the *distribution* of stellar ages does reflect that the disk of S1 formed inside-out. At $R \sim$ 5–6R_d, the fractions of stars younger than 3, 6 and 9 Gyr are $\sim$ 15, 30 and 60%.

The distribution of stellar ages in the disk of S2 reflects the outside-in formation of this disk. At $R \sim$ 5–6R_d, there are almost no stars with ages less than 3 Gyr, about 35% with ages less than 6 Gyr, and only about 10% with ages larger than 9 Gyr. The latter explains the slightly lower mean age of the outer disk of S2 compared to S1.

Ferguson & Johnson (2001) find in a recent observational study of the outskirts of M31's disk that the typical stellar age at $\sim$ 5–6 disk scale lengths is $\gtrsim$ 7–8 Gyr. This seems in fair agreement with our results on the mean stellar ages at $\sim$ 5–6 R_d, which are also lower limits since we have excluded all stars with $z_f > 2.6$. But at least in the disk of S1 we find a non-negligible fraction of stars younger than 3 Gyr in the outskirts of the disk — whether this is consistent with the observational findings of Ferguson & Johnson remains to be seen.

The mean age of the disk stars inside of $R = 6R_d$, with $z_f < 2.6$ and excluding the two innermost bins, which have some bulge contribution, is 7.3 Gyr for S1. This corresponds to a mean disk star formation redshift of $< z_f > \gtrsim$ 0.8, so for this galaxy even the formation of the bulk of the *stellar* disk happens at $z \sim 1$. For galaxy S2, the corresponding number is 4.9 Gyr, so for this galaxy the stellar disk is arguably still forming — its present SFR is also quite respectable, cf. Table 2.

Finally, our results above on age gradients indicate that the colour gradients observed in galactic disks (with the disk generally becoming bluer with increasing R) are a metallicity effect, rather than an age effect.

5.6. *Gas accretion histories for galactic disks and the "G-dwarf problem"*

Observational studies of the metallicity distribution of G and K stars in the solar neighbourhood show that the distribution is very narrow (peaking around [Fe/H]=–0.2 dex; Wyse & Gilmore 1995; Rocha-Pinto & Maciel 1996; Hou et al. 1998; Jørgensen 2000; Flynn & Morell 1997; Kotoneva et al. 2002), much too narrow to be consistent with what is expected from a simple, closed-box model of galactic chemical evolution. This famous, apparent inconsistency has been coined the "G-dwarf problem" and was first discussed by van den Bergh (1962), Schmidt (1963) and Pagel & Patchett (1975). The currently most popular (and very sensible — see below) answer to the G-dwarf problem is to assume that the solar neighbourhood was formed gradually over the Hubble time through prolonged infall of fairly low metallicity cooled-out gas originating from the hot halo; such "infall models" were first introduced by Larson (1972) and Lynden-Bell (1975). Assuming, as is often done for simplicity, that the infall rate is an exponentially decaying function of time an infall timescale of t_{inf}=7–10 Gyr is required to get the models to match recent observations (Chiappini et al. 1997; Portinari et al. 1998; Boissier & Prantzos 1999). If a gaussian form for the infall rate is assumed, then the typical timescale is $\sim$5 Gyr (Prantzos & Silk 1998; Chang et al. 1999). With the current models we are able to test these assumptions:

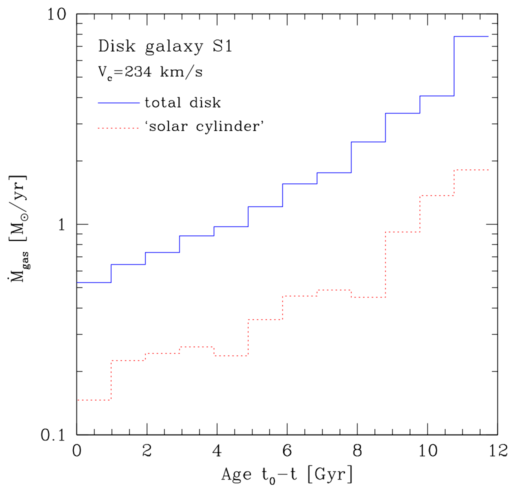

FIG. 20.— Rates of infall of cooled-out halo gas onto the disk of galaxy S1 versus age. Solid line: all disk, dotted line: "solar cylinder" (operationally defined as $2.1R_d \leq R \leq 3.2R_d$).

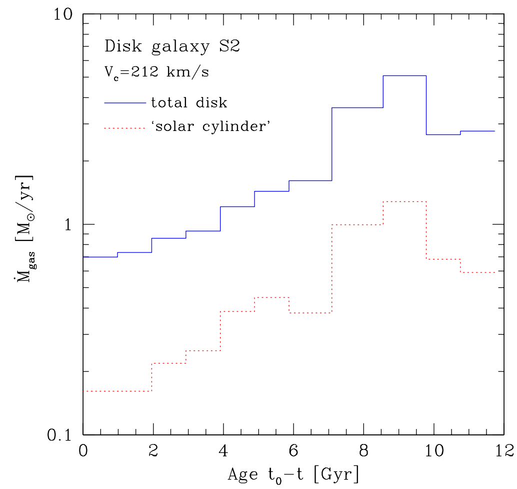

FIG. 21.— As Fig. 20, but for galaxy S2.

In Figure 20 and 21 we show the histories of accretion of cooled-out gas for the disks of galaxies S1 and S2, respectively. In each figure we show by solid line the accretion rate history of the entire disk and by dotted that of the "solar cylinder" (operationally defined as $2.1R_d \leq R \leq 3.2R_d$; we assume that the scalelength of the Galactic disk is 3.0 kpc, as a compromise between various recent determinations, and that the solar circle is at R_0=8.0 kpc). For S1 the rate of gas infall onto the "solar cylinder" is almost perfectly exponentially decaying with an e-folding time of $\sim$ 5 Gyr (the earliest bin in the figures correspond to z=2.2). For S2 the infall history looks more like the one derived by Prantzos & Silk (2003) for the solar cylinder using a combination of observational data and theoretical arguments. From a linear fit to the infall rate history of the "solar cylinder" over the age range 0–12 Gyr we derive an infall timescale of $\sim$ 6 Gyr. So the infall timescales derived fall short of the 7–10 Gyr required by current chemical evolution models, but only marginally so. Moreover, we remind the reader again that we have been analyzing just two Milky Way like disk galaxies in detail.

5.7. *Hot gas in galaxy haloes and pulsar dispersion measures*

The amount of hot gas ($T \sim 10^6$ K) in the Galactic halo can be constrained from dispersion measures to pulsars in the Galactic halo. Of particular interest is one pulsar in the high latitude globular cluster M53 and three in the LMC (Large Magellanic Cloud), because the distances to these pulsars are known. Rasmussen (2000) finds from these data and some modelling of the hot halo an upper limit on the cumulative amount of hot gas to the distance of the LMC of 1.5–2$\cdot 10^9$ $M_\odot$. In Figure 22 we show the cumulative mass of hot gas vs. galactocentric distance for three Milky Way like disk galaxies. Solid curves are for gas with $T > 10^5$ K, dotted for $T > 10^6$ K. Top set of curves are for disk galaxy S2, middle for S1 and lower are for a simulation of SPSF type of the halo corresponding to galaxy S1, but with a gas abundance of 1/3 solar (see Toft et al. 2002), rather than the primordial gas abundance used in this work. It is clear that all three hot gas haloes satisfy the above constraint increasingly so with increasing gas abundance, as discussed by Toft et al.

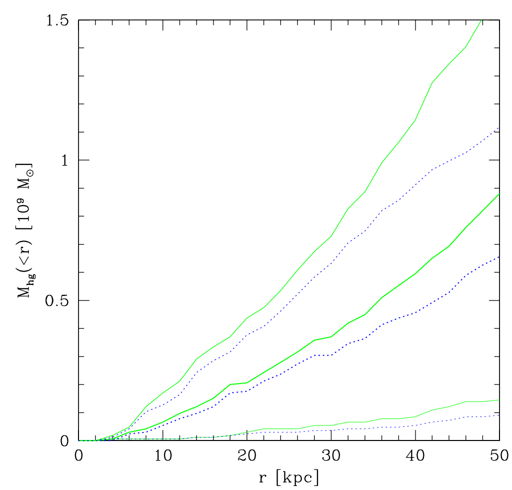

FIG. 22.— Cumulative mass of hot gas vs. galactocentric distance for three Milky Way like galaxies. Solid curves are for gas with $T > 10^5$ K, dotted for $T > 10^6$ K. Top set of curves are for disk galaxy S2, middle for S1 and lower are for a simulation of SPSF type of the halo corresponding to galaxy S1, but with a gas abundance of 1/3 solar (see Toft et al. 2002), rather than the primordial gas abundance used in this work.

With the present models we can, however, do better than this, because we can "insert" M53 and the LMC in our model galaxy haloes and calculate the expected dispersion measures directly:

For electromagnetic waves propagating through a plasma, the group velocity v_{gr} will depend on the fre-

quency ν of the radiation. Specifically, for radio waves in an unmagnetized plasma (e.g., Fälthammer 1995)

$$v_{gr} = c\sqrt{(1-\frac{\nu_{pe}^2}{\nu^2})} \ , \tag{8}$$

where $\nu_{pe} = (n_e e^2/\pi m_e)^{1/2}$ is the electron plasma frequency, e the electron charge, m_e the mass of the electron and c the speed of light. A pulse travelling a distance L in the plasma will have a travel time t given approximately by

$$t \approx \frac{L}{c} + \frac{e^2 D_m}{2\pi m_e c \nu^2} \tag{9}$$

rather than the "vacuum value" L/c (e.g., Spitzer 1978), where the *dispersion measure* D_m is defined as

$$D_m \equiv \int_0^L n_e dl \ \ . \tag{10}$$

Detected radio signals from pulsars show a frequency-dependent delay that can be used to evaluate D_m. For the pulsar in the globular cluster M53, located at a distance of $\approx$18.9 kpc at (l,b) = (333°,80°) one finds D_m=24.0 cm^{-3} pc. For the three pulsars in the LMC, located at a distance of $\approx$49.4 kpc at $(l,b) \simeq$ (279°,-33°), D_m=115±13 cm^{-3} pc is found (Rasmussen 2000).

To calculate what values of D_m we predict to M53 and the LMC for the haloes of S1 and S2 we average over the hot halo gas free electron densities in spherical shells and correct the densities for resolution effects at the disk-halo interface. We calculate D_m as the average of the value at z=0 and the values obtained at times 100 and 200 Myr prior to this. One has to adopt a value for R_0, the distance of the sun from the galactic center, when calculating D_m for the model galaxies. Though the *stellar* disks are too small compared to reality, this is not necessarily the case for the hot halo. We hence did the calculations of D_m with two values of R_0=5 and 8 kpc. For the M53 pulsar we find for S1 24±2 and 16±1 and for S2 28±1 and 17±1 cm^{-3} pc for R_0=5 and 8 kpc, respectively, in fairly good agreement with the observed value. For the LMC we find for S1 26±2 and 18±1 and for S2 31±1 and 20±1 cm^{-3} pc for R_0=5 and 8 kpc, respectively. These values are considerably smaller than the observed D_m — this is probably due to additional contributions to the observed D_m from the Gum Nebula, a largely ionized region at $l \sim$ 230°-290° and distance of about 0.5 kpc (Taylor & Cordes 1993), and the diffuse, ionized Reynolds-Layer (Reynolds 1993) in the direction towards the LMC (Rasmussen 2000).

It is clear from Fig. 22 and the discussion in Toft et al. (2002) that the predicted values of D_m above are upper limits in the sense that had we included chemical evolution in the simulations it would have lead to some non-zero level of metal enrichment in the hot halo gas, which in turn would have caused a reduction in the predicted values of D_m.

5.8. *Star formation histories*

As an example of the typical star formation histories in our simulations we show (for the *same* dark matter halo) in Figure 23 the star formation rate in units of the current one for three of the five simulations resulting in the largest disk galaxy (with $V_c \simeq$ 220–230 km/s). Two are with self-propagating star formation with $n_{H,e,low}$=0.05 and 0.25 cm^{-3} and one is for the simulation without self-propagating star formation. All three reproduce the observed peak in the SFR history at z∼2 (Madau et al. 1996), but whereas the simulations with self-propagating star formation have a low at z∼4.5–5.5 and another peak at z∼6–8 corresponding to the putative population III, the one without self propagating star formation has a monotonically decreasing SFR with increasing redshift. Though it would obviously be premature to take the star formation histories of our simulations of the formation and evolution of *individual* and fairly large galaxies as representative of the SFH of the Universe as a whole, our results suggest that the global SFH could possibly be bimodal. In relation to this it is interesting that recent observations of high-z quasars may indicate that the Universe was reionized at a redshift of about 6 (Becker et al. 2001; Djorgovski et al. 2001; but see also Hu et al. 2002, who advocate $z_{reion} \gtrsim$ 6.6 from observations of a candidate z=6.56 galaxy; this is, however, still consistent with the location of the second SFR peak discussed above). The different SFH scenarios should be observationally constrainable with upcoming instruments like JWST and ALMA.

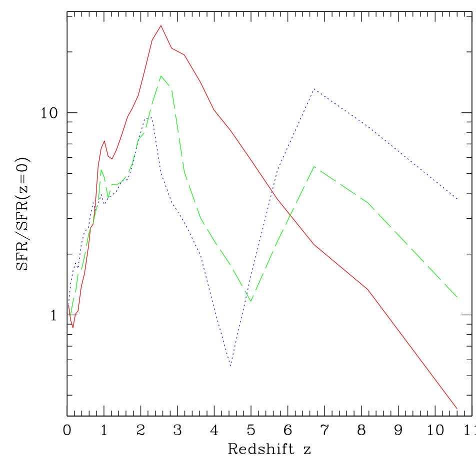

Fig. 23.— Star formation histories in three of the five of our simulations forming the largest disk galaxy (with $V_c \simeq$ 220-230 km/s). Two are for self-propagating star formation simulations with $n_{H,e,low}$=0.05 and 0.25 cm^{-3}, and are shown by dotted and dashed lines respectively. The last one is for the simulation without self-propagating star formation and is shown by the solid line.

5.9. *Effects of numerical resolution*

To check for effects of numerical resolution we did the following two tests:

1. We ran a series of 7 SPSF disk galaxy formation simulations with $n_{H,e,low}$=0.2 and with gravitational softening lengths equal to half the "standard" values, i.e. 0.65 h^{-1}kpc and 1.4 h^{-1}kpc for the SPH (and star) and active DM particles, respectively. The median normalized stellar specific angular momentum was 11±15% lower than for the "standard" simulations. This was mostly due to the median V_c being 4±12% larger than for the standard simulations. So there may be a small (and

statistically insignificant) effect of the gravitational softening on the resulting normalized specific angular momenta - but see below.

2. The second test was to re-simulate one of our disk galaxies, which we shall denote S3 in the following, at 8 times higher mass and 4 times higher force resolution, as detailed at the end of section 4. We shall denote the higher mass and force resolution version of S3 by S3-8 in the following. Masses, numbers of particles and other physical characteristics of S3 and S3-8 at z=0 are given in Tables 1 and 2. The total (baryonic) masses of S3 and S3-8 are very similar, differing by less than 5%. The stellar mass of S3-8 is 11% larger than that of S3 and the cold gas mass correspondingly smaller. We believe that it is the combination of the ability to resolve gas clouds of smaller masses and the additional small scale power that leads to the somewhat higher stellar mass and correspondingly lower cold gas mass of the high resolution galaxy S3-8 relative to S3. The characteristic circular speed of S3-8 is just 2% larger than that of S3 despite the 4 times higher force resolution. This may indicate that force resolution used in our "standard" simulations is adequate. The bulge-to-disk ratio of S3-8 is B/D=0.28±0.13. To obtain the j_* and R_d given in Table 2 for S3 we forced the bulge-to-disk decomposition to have B/D=0.28 for S3 to enable a fair comparison between S3 and S3-8. We find that j_* for S3-8 is 5±8% larger than that of S3 and that the specific angular momentum of the cold gas j_{cg} is 41% larger. The gas accretion rate is somewhat lower (this is presumably related to the larger stellar mass and smaller cold gas mass of S3-8 relative to S3) and the star formation rates and birthrate parameters, b, are very similar.

We conclude that the high mass resolution simulation generally is in good agreement with the "standard" resolution one, with a tendency for the stellar mass to be somewhat larger, the cold gas mass somewhat smaller and the specific angular momenta somewhat larger. All in all it is hence possible that increased mass resolution will be beneficial also with respect to the AM problem.

6. CONCLUSION AND OUTLOOK

In conclusion we have obtained a mix of realistic disk, lenticular and elliptical galaxies[1] in our ΛCDM galaxy formation simulations with effects of energetic stellar feedback processes included. We find that the disk galaxy angular momentum problem can be considerably alleviated (though not entirely solved as yet) in this way, provided that the early star-bursts are fairly strong, converting 2-5% of the initial gas mass into stars. For early starburst strengths in this range, the improvement on the AM problem is about the same, so extreme fine-tuning of the feedback seems not required.

The stellar disks have approximately exponential surface density profiles and those of the bulges range from exponential to $r^{1/4}$, as observed. The bulge-to-disk ratios of the disk galaxies are consistent with observations and likewise are their integrated B–V colours, which have been calculated in a simplified way ("post-process") using stellar population synthesis techniques. Furthermore we can match the observed I-band Tully-Fisher relation, provided that the stellar mass-to-light ratio of disk galaxies is $M/L_I \sim 0.8$, similar to what was found by Sommer-Larsen & Dolgov (2001) from their WDM simulations and in fair agreement with several recent observational determinations of M/L_I for disk galaxies.

The ellipticals and lenticulars have approximately $r^{1/4}$ stellar surface density profiles, are dominated by non disk-like kinematics and flattened due to non-isotropic, stellar velocity distributions, again consistent with observations.

We predict that hot halo gas is cooling out and being accreted onto the Galactic disk at a rate of 0.5–1 $M_\odot$/yr at z=0, consistent with upper limits deduced from *FUSE* observations of OVI. We have analyzed the formation history of two Milky Way like disk galaxies in detail and find gas accretion rates, and hence bolometric X-ray luminosities of the haloes, 6–7 times larger at $z \sim 1$ than at z=0 for these disk galaxies. More generally, we find that gas infall rates onto these disks are nearly exponentially declining with time, both for the total disk and the "solar cylinder". This theoretical result hence supports the exponentially declining gas infall approximation often used in chemical evolution models. The infall time-scales deduced are ∼5–6 Gyr, comparable to what is adopted in current chemical evolution models to solve the "G-dwarf problem".

It is moreover found for these two galaxies that galactic disks can form "inside-out" as well as "outside-in", but in both cases the mean ages of the stars in the outskirts of the disks are $\gtrsim$6–8 Gyr, broadly consistent with the findings of Ferguson & Johnson for the disk of M31.

The amount of hot gas in disk galaxy haloes is consistent with observational upper limits. We "insert" the globular cluster M53 and the LMC in the haloes of the two Milky Way like disk galaxies and calculate dispersion measures to these objects. Our results are consistent with upper limits from observed dispersion measures to pulsars in these systems.

Our simulations indicate that we can reproduce the observed peak in the cosmic star formation rate at redshift $z \sim 2$. Depending on the star formation and feedback scenarios we predict either a monotonically decreasing cosmic star formation rate beyond these redshifts or a second peak at z∼6–8 corresponding to the putative population III and interestingly similar to recent estimates of the redshift at which the Universe was reionized. These various scenarios should hence be observationally constrainable with upcoming instruments like JWST and ALMA.

In this paper we have mainly been concerned with the present day properties of the simulated disk galaxies. We shall in forthcoming papers study the present day properties of the E/S0s in detail as well as the dynamics of all types of galaxies. In particular, we intend to study the kinematics and dynamics of the stellar haloes of Milky Way like disk galaxies to compare with current models of the Galactic stellar halo (e.g., Sommer-Larsen et al. 1997; Helmi & White 1999; Helmi et al. 1999). We will also study the higher redshift properties of all types of galaxies and the properties of medium to high-z damped Lyα systems predicted by our simulations. Moreover, we will incorporate chemical evolution including non-instantaneous gas and heavy element recycling in the

[1] Pictures of some of the galaxies can be seen at http://www.tac.dk/~jslarsen/Hubble_Sequence

simulations and replace thermal energy by entropy as an independent variable in SPH (Springel & Hernquist 2002).

Last, but not least we will also study much more closely the physical factors determining the final Hubble type of the galaxies formed. It is, however, already at this point clear from our simulations that final galaxy morphologies primarily reflect the merging histories of the galaxies in the sense of the very *detailed* merging histories — just to give an example, we find that even major merging sometimes can be *constructive* in forming disk galaxies with extended disks. Another interesting result is that whereas the mean spin-parameter for the 5 spheroid dominated systems (E/S0) is $<\lambda_{200}>_{E/S0}$=0.043±0.005, it is $<\lambda_{200}>_S$=0.037±0.002 for the 35 disk galaxies. Hence our results do not seem to support the notion that the DM haloes in which disk galaxies form on average have larger spin-parameters than the haloes of early type galaxies (e.g., Mo, Mao & White 1998; van den Bosch 1998).

We have benefited from discussions with G. Bryan, Y.-I. Byun, G. Carraro, C. Chiappini, C. Chiosi, P. R. Christensen, R. Dominguez-Tenreiro, A. Ferguson, C. Flynn, K. Freeman, J. Hjorth, R. Kennicutt, A. Kravtsov, C. Lia, F. Matteucci, J. Monaghan, B. Moore, Å. Nordlund, B. Pagel, K. Pedersen, N. Prantzos, V. Quilis, J. Rasmussen, A. Saiz, B. Savage, V. Springel, S. Toft, G. Yepes, S. Yi and, in particular, Joe Silk. The comments by the anonymous referee significantly improved the presentation of our results. LP acknowledges kind hospitality from the Astronomy Department of Padua and from the Observatory of Helsinki. JSL acknowledges the help by A. Sommer-Larsen and M. Vestergård in analyzing the observational data used in this paper. This work was supported by Danmarks Grundforskningsfond through its support for the establishment of the Theoretical Astrophysics Center.

REFERENCES

Abadi, M.G., Navarro, J.F., Steinmetz, M., Eke, V.R. 2003, ApJ, 591, 499
Abel, T., Bryan, G.L., & Norman, M.L. 2002, Science 295, 93
Balsara, D. S. 1995, J. Comp. Phys., 121, 357
Barnes, J., & Efstathiou, G. 1987, ApJ, 319, 575
Bate, M.R., & Burkert, A. 1997, MNRAS, 288, 1060
Becker, R. H., et al. 2001, AJ, 122, 2850
Boissier, S., & Prantzos, N. 1999, MNRAS, 307, 857
Bromm V., Coppi P. S., & Larson R. B. 2002, ApJ, 564, 23
Bryan, G. L. 1999, Computing in Science and Engineering, 1:2, 46
Bryan, G. L. 2003, in preparation
Byun, Y-I., 1992, PhD thesis, The Australian National University
Chabrier G. 2003, PASP, 115, 763
Chang R.X., Hou J.L., Shu C.G., & Fu C.Q. 1999, A&A, 350, 38
Charlot, S., & Fall., S.M. 2000, ApJ, 539, 718
Charlot, S., Worthey, G., & Bressan, A. 1996, ApJ, 457, 625
Chiappini C., Matteucci F., & Gratton R.G. 1997, ApJ, 477, 765
Chiosi C. 2000, Proceedings of the MPA/ESO Workshop on The First Stars, A. Weiss, T. Abel and V. Hill eds., ESO Astrophysics Symposia, Springer, p. 137
Couchman, H. M. P., Thomas, P. A., & Pearce, F. R. 1995, ApJ, 452, 797
de Jong, R. S. 1996, A&A, 313, 45
Dekel, A., & Silk, J. 1986, ApJ, 303, 39
Djorgovski, S. G., Castro, S., Stern, D., & Mahabal, A. A. 2001, ApJ, 560, L5
Edgar, R. J., & Chevalier, R. A. 1986, ApJ, 310, L27
Eke, V. R., Cole, S., & Frenk, C. S. 1996, MNRAS, 282, 263
Eke, V. R., Efstathiou, G., & Wright, L. 2000, MNRAS, 315, L18
Ettori, S., & Fabian, A.C. 1999, MNRAS, 305, 834
Fall, S. M. 2002, in *The Dynamics, Structure & Evolution of Galaxies*, eds. G. S. Da Costa & E. M. Sadler ASP Conf. Series 273, 289
Fall, S. M., & Efstathiou, G. 1980, MNRAS, 193, 189
Fälthammer, C.-G. 1995, *Space Physics*, Royal Institute of Technology, Stockholm
Ferguson, A. M. N., & Johnson, R. A. 2001, ApJ, 559, L13
Ferrara, A., & Tolstoy, E. 2000, MNRAS, 313, 291
Flynn C., & Morell, O. 1997, MNRAS, 286, 617
Gelato, S., & Sommer-Larsen, J. 1999, MNRAS, 303, 321
Gerritsen, J. P. E. 1997, Ph.D. thesis, Kapteyn Astron. Inst.
Giovanelli, R., et al. 1997a, ApJ, 477, L1
Giovanelli, R., et al. 1997b, AJ, 113, 53
Governato, F., et al. 2002, ApJ, submitted (astro-ph/0207044)
Haardt, F., & Madau, P. 1996, ApJ, 461, 20
Heavens, A., & Peacock, J. 1988, MNRAS, 232, 339
Helmi, A., & White, S. D. M. 1999, MNRAS, 307, 495
Helmi, A., White, S. D. M., de Zeeuw, P. T., & Zhao, H. 1999, Nature, 402, 53
Hernquist, L., & Katz, N. 1989, ApJS, 70, 419
Hou J., Chang R., & Fu C. 1998, ASP Conf. Series 138, 143
Hu, E. M., et al. 2002, ApJ, 568, L75
Jørgensen B.R. 2000, A&A, 363, 947
Katz, N. 1992, ApJ, 391, 502
Kennicutt, R. C. 1998, ApJ, 498, 541
Kennicutt, R. C., Tamblyn, P., & Congdon, C. W. 1994, ApJ, 435, 22
Kodama, T., & Arimoto, N. 1998, MNRAS, 300, 193
Kotoneva, E., Flynn, C., Chiappini, C., & Matteucci, F. 2002, MNRAS, 336, 879
Kroupa, P., Tout, C.A., & Gilmore, G. 1993, MNRAS, 262, 545
Kudritzki R. P. 2002, ApJ, 577, 389
Kudritzki R. P. & Puls J. 2000, ARA&A, 38, 613
Kudritzki R. P., Pauldrach A. W. A., Puls J. & Abbott D. C. 1989, A&A, 219, 205
Larson R.B., 1972 Nat. Phys. Sci., 236, 7
Lia, C., Portinari, L., & Carraro, G. 2002, MNRAS, 330, 821
Lynden-Bell, D. 1975, Vistas in Astronomy, 19, 299
Mac Low, M.-M. & Ferrara, A. 1999, ApJ, 513, 142
Madau, P., et al. 1996, MNRAS, 283, 1388
Mathewson, D. S., Ford, V. L., & Buchhorn, M. 1992, ApJS, 81, 413
McCray, R., & Kafatos, M. C. 1987, ApJ, 317, 190
Meza, A., Navarro, J.F., Steinmetz, M., Eke, V.R. 2003, ApJ, 590, 619
Mo, H. J., Mao, S., & White, S. D. M. 1998, MNRAS, 295, 319
Monaghan, J. J., & Gingold, R. A. 1983, J. Comput. Phys., 52, 374
Monaghan, J. J., & Lattanzio, J. C. 1985, A&A, 149, 135
Mori, M., Yoshii, Y., Tsujimoto, T., & Nomoto, K. 1997, ApJ, 478, L21
Navarro, J. F., & Benz, W. 1991, ApJ, 380, 320
Navarro, J. F., & White, S. D. M. 1994, MNRAS, 267, 401
Navarro, J. F., Frenk, C. S., & White, S. D. M. 1995, MNRAS, 275, 56
Navarro, J. F., & Steinmetz, M. 1997, ApJ, 478, 13
Navarro, J. F., & Steinmetz, M. 2000, ApJ, 528, 607
Padoan, P., & Nordlund, Å. 2002, ApJ, 576, 870
Pagel, B. E. J. 1997, Nucleosynthesis and Chemical Evolution of Galaxies, Cambridge University Press
Pagel, B. E. J. 2002, in Chemical Enrichment of the Intracluster Medium, F. Matteucci and F. Giovanelli eds., ASP Conf. Ser., 253, p. 429
Pagel B.E.J., & Patchett B.E. 1975,MNRAS, 172, 13
Portinari, L., Chiosi, C., & Bressan, A. 1998, A&A, 334, 505
Portinari, L., Sommer-Larsen, J., & Tantalo, R. 2003, MNRAS, in press (astro-ph/0303190)
Prantzos N., & Silk J. 1998, ApJ, 507, 229
Prantzos N., & Silk J. 2003, in preparation
Rasmussen, J. 2000, Master Thesis, University of Copenhagen

Reynolds, R. J. 1993, in *Back to the Galaxy*, eds. S. Holt & F. Verter (New York: American Institute of Physics), p. 156
Renzini A., & Buzzoni A. 1986, in Spectral Evolution of Galaxies, C. Chiosi and A. Renzini eds., Dordrecht, Reidel pub., p. 195
Roberts, M., & Haynes, M. 1994, ARA&A, 32, 115
Rocha-Pinto H.G., & Maciel W.J. 1996, MNRAS, 279, 447
Savage, B. D. et al. 2003, ApJS, 146, 125
Schmidt, M. 1963, ApJ, 137, 758
Semelin, B., & Combes, F. 2002, A&A, 388, 826
Silk, J. 1997, ApJ, 481, 703
Silva, L., Granato, G.L., Bressan, A., & Danese, L. 1998, ApJ, 509,103
Simard, L., et al. 1999, ApJ, 519, 563
Sommer-Larsen, J. 1991, MNRAS, 250, 356
Sommer-Larsen, J., 1996, ApJ, 457, 118
Sommer-Larsen, J., & Dolgov, A. 2001, ApJ, 551, 608 (SLD01)
Sommer-Larsen, J., Beers, T.C., Flynn, C., Wilhelm, R., & Christensen, P. R. 1997, ApJ, 481, 775
Sommer-Larsen, J., Gelato, S., & Vedel. H. 1999, ApJ, 519, 501 (SLGV99)
Sommer-Larsen, J., Vedel, H., & Hellsten, U. 1998, ApJ, 500, 610
Sommer-Larsen, J., Vedel, H., & Hellsten, U. 1998, MNRAS, 294, 485
Sommer-Larsen, J., Beers, T.C., Flynn, C., Christensen, P.R., Portinari, L. 2003, in preparation
Spitzer, L. 1978, *Physical Processes in the Interstellar Medium*, Wiley, New York
Springel, V., & Hernquist, L. 2002, MNRAS, 333, 649
Springel, V., & Hernquist, L. 2003, MNRAS, 339, 289
Springel, V., Yoshida, N. & White, S.D.M. 2001, NewA, 6, 79
Steinmetz, M., & Navarro, J. F. 2002, New Astronomy, 7, 155
Sutherland, R. S., & Dopita, M. A. 1993, ApJS, 88, 253
Tantalo, R., Chiosi, C., Bressan, A., & Fagotto, F. 1996, A&A, 311, 361
Taylor, J. H., & Cordes, J. M. 1993, ApJ, 411, 674
Thacker, R. J., & Couchman, H. M. P. 2001, ApJ, 545, 728
Thacker, R. J., & Couchman, H. M. P. 2001, ApJ, 555, L17
Tinsley, B.M. 1980, Fund. Cosmic Phys., 5, 287
Toft, S., Rasmussen, J., Sommer-Larsen, J., & Pedersen, K. 2002, MNRAS, 335, 799
Tosi, M. 1988, A&A, 197, 47
Trott, C.M., & Webster, R. L. 2002, MNRAS, 334, 621
Vallejo, O., Braine, J., & Baudry, A. 2002, A&A, 387, 429
van den Bergh S. 1962, AJ, 67, 486
van den Bosch, F. C. 1998, ApJ, 507, 601
van der Kruit, P. C., & Searle, L. 1982, A&A, 110, 61
Vedel, H., Hellsten, U., & Sommer-Larsen, J. 1994, MNRAS, 271, 743
Weil, M. L., Eke, V. R., & Efstathiou, G. 1998, MNRAS, 300, 773
White, S. D. M., & Frenk, C. S. 1991, ApJ, 379, 52
Wolfe, A. M., Turnshek, D. A., Smith, H. E., & Cohen, R. D. 1986, ApJS, 61, 249
Wyse R.F.G., Gilmore G. 1995, AJ, 110, 2771
Yepes, G., Kates, R., Khokhlov, A., & Klypin, A. 1997, MNRAS, 284, 235
Yoshii, Y., & Arimoto, N. 1987, A&A, 188, 13